Modeling prey-predator interactions in Messina beachrock pools

S. Savoca[(1)], G. Grifó[(2,*)], G. Panarello[(1)], M. Albano[(1)], S. Giacobbe[(1)], G.Capillo[(3)], N. Spanó[(4)], G. Consolo[(2)]

[(1)] Department of Chemical, Biological, Pharmaceutical and Environmental Sciences University of Messina (Italy), V.le F. D'Alcontres 31, I-98166 Messina, Italy.

[(2)] Department of Mathematical, Computer, Physical and Earth Sciences University of Messina (Italy), V.le F. D'Alcontres 31, I-98166 Messina, Italy.

[(3)] Department of Veterinary Sciences, University of Messina (Italy), Polo Universitario dell'Annunziata, I-98168 Messina, Italy.

[(4)] Department of Biomedical, Dental and Morphological and Functional Imaging University of Messina (Italy), Via Consolare Valeria, I-98124 Messina, Italy

[(*)] Corresponding author: gabgrifo@unime.it.

Abstract

The Strait of Messina (Sicily, Italy) attracts the interest of marine ecologists for the presence of a large variety of habitat and mutually-interacting communities. Among them, beachrock formations, despite their wide geographic distribution, which also includes the Mediterranean area, have been poorly investigated from the biotic viewpoint. In this paper, the spatial and seasonal variability of benthic megafauna from the Messina microtidal beachrock is described. Combining *in situ* collected data (measurements of abiotic parameters and underwater visual census) with theoretical post-processing analyses (analysis of similarity percentages and cluster analysis), we deduced the possibility to model the dynamics observed between the most dominant species, a top snail, *Phorcus turbinatus* (Born, 1778), and a hermit crab, *Clibanarius erythropus* (Latreille, 1818), in terms of a prey-predator interaction. These species gave rise to different intriguing dynamical regimes (including periodic oscillations) that were qualitatively captured by a mathematical model focused on the respective trophic chain levels. The identification of all model parameters and the use of numerical simulations complemented the above analysis and allowed to gain more insights into the complex dynamics of these oligotypic communities and on the most relevant factors determining the ecosystem equilibria.

Keywords: prey-predator interaction, beachrock, marine ecology, Hopf bifurcation, carrying capacity, benthic community

1 Introduction

Interaction among species, populations and communities are at the base of ecosystem equilibria [1, 2]. Among the different interactions, the prominent role played by prey-predator relationships is basic to gain an understanding on ecosystem dynamics [3].

Prey-predator interaction is a well-known topic, both in wild and experimental conditions. In wild environments it involves several behavioral strategies, such as selection of prey according to suitable morphological and behavioral features, detection and capture, camouflage, cooperation and defense mechanisms (e.g. release of repulsive chemical compounds, evasive movements, etc.).

In a natural environment, the interaction between two species can be hard to determine, due to the numerous factors affecting the whole ecosystem balance [4]. This is especially true in high biodiversity areas characterized by a rich variety of mutually-interacting plant and animal communities.

The Strait of Messina (Sicily, Italy), known for the peculiar and diversified marine habitats [5, 6], includes a long-shore rocky structure known as "Messina beachrock"that represents, in this respect, an appropriate case-study [7]. Such worldwide distributed structure may occur from the intertidal to the upper subtidal zone [8, 9] and are characterized by large fluctuations of both biotic and abiotic conditions due to, for example, tidal cycles and storms [10, 11, 12]. Messina beachrock, preliminary described in [13], is characterized by a microtidal regime, similar to that encountered in other known formations, e.g., in eastern Mediterranean [14]. The interest in studying such zones also arises from the fact that they represent sensitive indicators of the effects of climate change in coastal ecosystems [15, 16, 17, 18].

The species inhabiting these extreme environments need morphological, physiological and behavioral adaptations [19]. Consequently, settled communities are markedly oligotypic. In this ultra-simplified context, some evidences of prey-predator interactions between benthic species have been preliminary reported [20]. The case-study concerns the top-snail, *Phorcus turbinatus* (Born, 1778), and the hermit crab, *Clibanarius erythropus* (Latreille, 1818). Indeed, it is known that this latter feeds upon the gastropod and steals the molluscan shell as an additional protection against predators [21].

The present study aims at elucidating some ecosystem dynamics taking place in the peculiar beachrock formation. In particular, the main goals are: (i) to describe the local megabenthic communities; (ii) to individuate possible prey-predator dynamics on the basis of the analysis of the factors influencing and determining organisms distribution and abundance; (iii) to theoretically describe such prey-predator interactions through a mathematical model able to qualitatively capture the most relevant behavioral aspects.

The paper is organized as follows. In Section 2, details on the investigated area, sampling methodology, variables, statistical tools used in data analysis, mathematical model and numerical simulations tools are provided. In particular, we discuss a simple prey-predator model and address a linear stability analysis to determine the local stability character of the equilibria against small perturbations as well as to explore the occurrence of Hopf bifurcation responsible for oscillatory behaviors. In Section 3, results of statistical analysis on ecological parameters are exposed, the outcome of visual census procedure is discussed, a multivariate analysis is performed and the occurrence of possible prey-predator interactions is assessed. In the same section, the different dynamical regimes observed *in situ* are mathematically described, all the model parameters are identified and numerical simulations are carried out to qualitatively reproduce the various population dynamics that followed one another throughout the sampling period. Discussions on ecological implications, mathematical

assumptions and future developments of this work are reported in the last section.

2 Materials and methods

In this section, we first briefly describe the investigated habitat. Then, the experimental and statistical tools adopted in the post-processing analyses are illustrated.

2.1 Study Area and sampling design

The strait of Messina directly connects the Ionian and Tyrrhenian basins that, in spite of being geographically contiguous, are dissimilar for physical, chemical and oscillatory water characteristics as well as for shape and bathymetry. Such structural heterogeneity is responsible for a complex patchiness of different habitats [6, 22], coupled with migratory processes of species belonging to different trophic levels [23].

Along the northern Messina's coast, a peculiar beachrock formation extends between the narrow intertidal zone and the upper subtidal fringe. The sub-horizontal upper surface includes numerous irregular rocky pools, more or less connected with the sea and substantially unaffected by the local microtidal regime [24]. The study area ranges between the coordinates 38°25′69″ N, 15°61′24″ E and 38°15′43″ N, 15°38′13″ E and is part of the Oriented Natural Reserve of Capo Peloro (Messina, Italy) [25]. Six randomly-selected stations, numbered from 1 (northernmost) to 6 (southernmost), have been monitored, each of them covering an area of about 190 m^2, to reach an overall monitored area of about 1148 m^2 (Fig.1) [20].

In order to acquire a significant amount of data needed to formulate a mathematical description, the sampling activity through visual census was carried out for more than one year: from October 2016 to January 2018. Samplings were performed with variable periodicity: from two days to about two weeks, depending on weather conditions.

2.2 Water variables

The main water variables, Temperature (°C), Salinity (PPT) and pH, were measured *in situ*, using a multi-parametric probe IM201 (Idromar s.r.l., Milano, Italy) [26].

2.3 Underwater Visual Census

Among the different Underwater Visual Census (UVC) methods, we chose the survey based on on-site visual counts of organisms with the help of a pre-measured rope. Considering the low-depth of the transects, the usual UVC snorkeling method was replaced by the use of a glass screen that allowed the operator to perform the visual analysis in standing position, inspecting the beachrock area from above the water surface.

2.4 Data analysis

Data analysis was performed by using a combination of univariate and multivariate statistical methods. Regarding environmental parameters, One-way ANOVA analysis was performed to assess spatial and temporal significant differences.

Figure 1: Left figure: Strait of Messina, Sicily, Italy. Right figures: zooms over some beachrock areas. Bottom figure: an overview of the location of the six stations.

The macrobenthic community structure was analyzed by taking into account macrofauna abundance (individuals/m^2) [27], number of taxa (S), Pielou's evenness index (J') and Shannon-Wiener's species diversity index (H'). These biological parameters were calculated for each station and season by using Past 2.7 [28]. The seasonal and spatial differences of indices were tested through one-way ANOVA, performing a post-hoc Tukey's Honestly Significant Difference (HSD) test when significant differences were found ($p < 0.05$) (Sigmaplot V.12).

Information on macrobenthic community was extracted through multivariate data analysis. A square root transformation was applied to the abundance matrix, then the Bray-Curtis similarities were calculated. At last, the dendrogram was created by means of the average linkage clustering method.

Non-parametric multi-dimensional scaling (nMDS) ordination was applied to the abundance matrix in order to detect spatial and temporal changes in the structure of macrobenthos community. The SIMilarity PERcentages (SIMPER) routine was used to establish which species contributed most to the observed differences in the data. Environmental variables which best correlated with the multivariate pattern of the macrobenthic community were identified by means of BIO-ENV procedure. All multivariate statistical analyses were performed by using PRIMER6-E.

2.5 Mathematical model

The visual census procedure described in Section 2.3 shed light on the most representative species inhabiting Messina's beachrock pools and, as a consequence of that, on the existence of possible interactions of prey-predator type occurring between them. These interactions were also investigated theoretically through a mathematical model. The aim of the proposed model is manifold: (i) providing a qualitative description of the most intriguing dynamics observed when the ecosystem is reduced to a simplified two-levels trophic chain, (ii) providing a quantitative estimation of the key model parameters and (iii) inferring temporal variations of model parameters, as a result of occurrence of different ecological scenarios.

To achieve these goals, we took into account a model describing the time evolution of the density of predators and preys as follows [29]:

$$\begin{cases} \frac{dP}{dt} = \beta P\left(1 - \frac{P}{k}\right) - h(P)C = f(P,C), \\ \frac{dC}{dt} = \epsilon\left(h(P) - m\right)C = g(P,C). \end{cases} \tag{1}$$

Here $P(t)$ and $C(t)$ denote, respectively, the densities (number of species per square meter) of preys and predators at time t. The prey growth was assumed to take a standard logistic form with β the intrinsic growth rate and k the carrying capacity density, whereas predation follows a Holling type-III "functional response"(FR), namely

$$h(P) = \frac{\lambda P^2}{\mu^2 + P^2}, \tag{2}$$

with the parameters λ and μ denoting the maximum predator grazing rate and the half-saturation constant for grazing, respectively. Predator mortality was here considered linear, with ϵm the mortality rate, where the coefficient $\epsilon < 1$ represents the predator growth efficiency. Owing to their biological meaning, all the above parameters $\beta, k, \lambda, \mu, \epsilon, m$ are real and positive.

The model (1) admits three equilibrium states in the form $E^* = (P^*, C^*)$ given by:

$$\begin{aligned} E_1^* = (0,0) \quad &\Longrightarrow \quad \text{the trivial state (empty ecosystem)} \\ E_2^* = (k,0) \quad &\Longrightarrow \quad \text{the predator-free state} \\ E_3^* = (P_3^*, C_3^*) \quad &\Longrightarrow \quad \text{the co-existence state} \end{aligned} \tag{3}$$

being

$$P_3^* = \mu\sqrt{\frac{m}{\lambda - m}} \tag{4}$$

and

$$C_3^* = \frac{\beta}{m} P_3^* \left(1 - \frac{P_3^*}{k}\right). \tag{5}$$

While the trivial state E_1^* and the predator-free state E_2^* exist for any set of parameter values, the co-existence state E_3^* is meaningful only if the parameter related to predator mortality m is smaller than the critical value $m_{cr} = \frac{\lambda k^2}{\mu^2 + k^2}$.

Hereafter we consider the coefficient m as the main control parameter as it encloses all those (intrinsic and extrinsic) effects that contribute in affecting predators' mortality rate. Among the most relevant factors causing fluctuations of the mortality rate, there are: characteristics of the

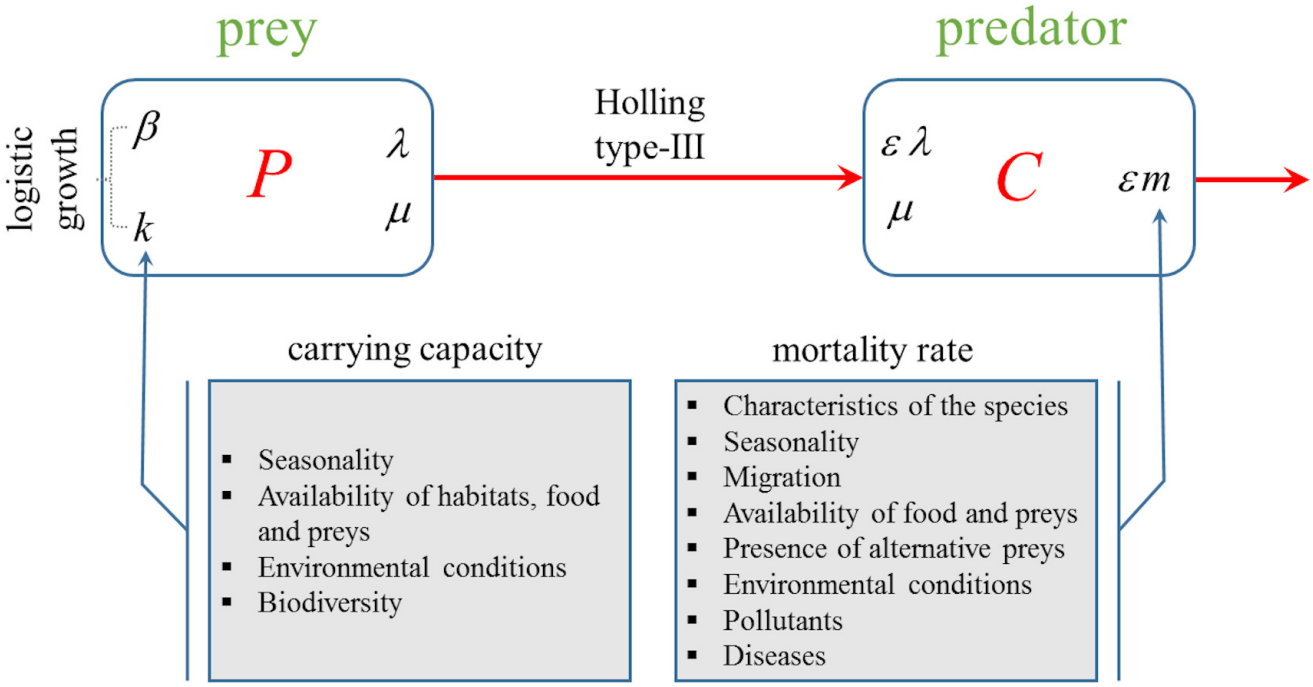

Figure 2: Simple conceptual scheme of the prey-predator model given in (1) with Holling type-III functional response. The rounded boxes represent state variables, whereas the squared boxes summarize the main factors causing fluctuations of the two control parameters.

species (*e.g.*, reactions to predators, stimulus detected by its predator); seasonality; migration; density and quality of alternate foods available for its predator; prey and predator's food preferences; availability of preys/nutrients; environmental conditions; pollutants, diseases and hydra effects [30],[31],[32],[33],[34].

Moreover, as widely discussed in the literature, the carrying capacity k is another key quantity that may be subject to temporal variability. Indeed, the carrying capacity of a given ecosystem is strongly dependent on several factors, such as seasonality, environmental conditions, biodiversity, hydrodynamical regime, water temperature, flow, availability of habitat, food and preys [35, 36, 37, 38]. On the other hand, despite the carrying capacity usually provides a measure of the number of individuals that the environment "can support" in a given area, many mechanisms may determine the presence of overshoots, such as decrease in biodiversity and/or trophic cascade/interactions, ecosystem instability [37]. As a consequence of the above considerations, we assume k as secondary control parameter. A conceptual diagram summarising the key assumptions of model (1) is given in Fig.2.

In order to inspect the stability character of the above equilibria (3), we linearize system (1) around E^* for small spatially-homogeneous time-dependent perturbations in the form $e^{\omega t}$, with ω the growth factor [39]. We get the following characteristic equation:

$$\omega^2 - (f_P^* + g_C^*)\,\omega + f_P^* g_C^* - f_C^* g_P^* = 0, \tag{6}$$

where the subscripts denote partial derivatives with respect to the indicated variables and the aster-

isks indicate that those functions are evaluated at E^*. As is known, a steady state is asymptotically stable if, and only if, all the eigenvalues ω of (6) exhibit negative real part. This is ensured if:

$$\begin{cases} f_P^* + g_C^* < 0, \\ f_P^* g_C^* - f_C^* g_P^* > 0. \end{cases} \tag{7}$$

Results of this analysis indicate that the trivial state E_1^* is always unstable, being

$$f_P(E_1^*) = \beta, \quad f_C(E_1^*) = 0, \quad g_P(E_1^*) = 0, \quad g_C(E_1^*) = -\epsilon m, \tag{8}$$

so that the condition $(7)_2$ is never fulfilled.

Regarding E_2^*, we have:

$$f_P(E_2^*) = -\beta, \quad f_C(E_2^*) = -\frac{\lambda k^2}{\mu^2 + k^2}, \quad g_P(E_2^*) = 0, \quad g_C(E_2^*) = \epsilon \left(\frac{\lambda k^2}{\mu^2 + k^2} - m \right), \tag{9}$$

so that the predator-free state is asymptotically stable if $m > m_{cr}$, *i.e.* prey population can stay at its carrying capacity value if the predator mortality exceeds a critical value. Notice that the predator-free state is stable in the region of the control parameter where the coexistence state E_3^* does not exist.

Finally, by evaluating the partial derivatives of the source terms with respect to the field variables at E_3^*:

$$\begin{aligned} f_P(E_3^*) &= \tfrac{\beta}{k\lambda} \left[k\,(2m - \lambda) - 2\mu m \sqrt{\tfrac{m}{\lambda - m}} \right], \quad f_C(E_3^*) = -m, \\ g_P(E_3^*) &= \tfrac{2\epsilon\beta(\lambda - m)}{\lambda} \left(1 - \tfrac{\mu}{k} \sqrt{\tfrac{m}{\lambda - m}} \right), \qquad g_C(E_3^*) = 0, \end{aligned} \tag{10}$$

we can conclude that the stability of the coexistence state also depends on the value of the carrying capacity k. In particular, E_3^* is asymptotically stable:

$$\begin{aligned} &\text{for } k < k_{min} \implies \text{always}, \\ &\text{for } k \geq k_{min} \implies \text{if } m \in \left(0, m_1^H\right) \cup \left(m_2^H, m_{cr}\right), \end{aligned} \tag{11}$$

being $k_{min} = \sqrt{27}\mu$. In (11), m_1^H and m_2^H, with $m_1^H < m_2^H$, are the two positive real solutions of the equation

$$4\left(\mu^2 + k^2\right) m^3 - 8\lambda k^2 m^2 + 5\lambda^2 k^2 m - \lambda^3 k^2 = 0 \tag{12}$$

that belong to the interval $m_{1,2}^H \in \left(\frac{\lambda}{2}, \frac{\lambda k^2}{4\mu^2 + k^2} \right)$.

It can be verified that, for $k = k_{min}$, the above roots coincide with each other, $m_1^H = m_2^H = m^H$, so that in this case E_3^* is stable for $m \neq m^H$.

The previous results indicate that there exists a critical value of the carrying capacity, $k = k_{min}$, below which the steady state E_3^* is always stable, as illustrated in Fig.3(b). Therefore, when the environment can sustain a relatively small prey population size ($k < k_{min}$) and the predator mortality is not so large ($m < m_{cr}$), the coexistence state represents the only stable state admitted by the system. On the contrary, when the critical value of carrying capacity is exceeded ($k > k_{min}$), the coexistence state may lose its stability depending on predator's mortality value m. In fact, for $m_1^H < m < m_2^H$, the characteristic polynomial (6) admits a couple of complex-conjugate roots with

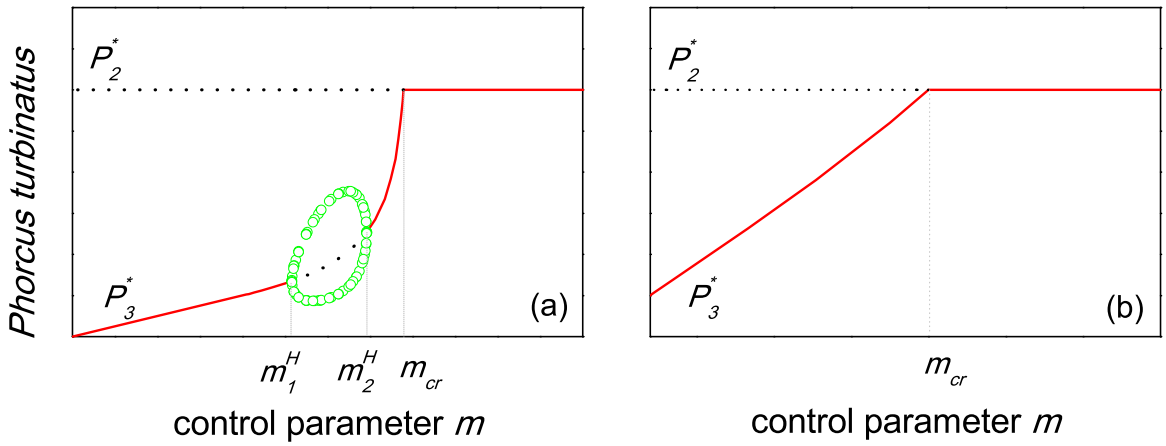

Figure 3: Bifurcation diagrams for density P with m the main control parameter, $k \geq k_{min}$ in (a) and $k < k_{min}$ in (b). Circles denote stable periodic solutions whereas solid (dotted) lines represent stable (unstable) stationary solutions.

positive real part. At the critical values $m = m^H_{1,2}$, the state E^*_3 becomes neutrally stable since eq.(6) admits a couple of complex-conjugate eigenvalues with null real part. At such critical values of the predator mortality, since the transversality condition

$$\left.\frac{\mathrm{d}Re\{\omega\}}{\mathrm{d}m}\right|_{m^H_{1,2}} = \frac{\beta\left(3\lambda - 4m^H_{1,2}\right)}{4m^H_{1,2}\left(\lambda - m^H_{1,2}\right)} \neq 0 \tag{13}$$

is fulfilled, the system undergoes a Hopf bifurcation that can be observed in the bifurcation diagram in Fig.3(a). The occurrence of a Hopf bifurcation for a given combination of carrying capacity and predator mortality implies the existence of a limit cycle that, at experimental level, manifests itself as a periodic behavior of the interacting species around their equilibrium population. At the onset of bifurcation, the period of such oscillations T is given by:

$$\frac{2\pi}{T} = \sqrt{\left|f^*_P g^*_C - f^*_C g^*_P\right|}. \tag{14}$$

2.6 Numerical tools

The analysis was complemented by numerical simulations used to systematically analyse how the system responses to perturbation of model parameters as well as to develop hypotheses useful to gain a deeper understanding on the underlying ecological processes.

Simulations were carried out by integrating numerically the governing system (1), together with assigned initial conditions, by means of two different numerical tools: MATLAB® (*ode23s* and *ode45* solvers) and XPPAUT 8.0 [40].

3 Results

In this section we report the outcomes of *in situ* measurements and theoretical investigations. In particular, we inspect temporal and spatial variations of abiotic parameters and of the main biological indexes characterizing the macrofaunal community. Then we address a multivariate analysis aimed at evaluating the most statistically significant species inhabiting Messina beachrock pools. Finally, we provide a mathematical description of prey-predator interactions, carry out the identification of all the model parameters and show the results of numerical simulations.

3.1 Abiotic parameters

Results of our investigations revealed that temperature, salinity and pH do not exhibit spatial variations, as reported in Table 1. None of the environmental variables showed indeed significant differences among stations ($p > 0.05$). On the contrary, temperature and pH exhibited significant seasonal variations ($p < 0.001$).

		Stations					
		1	**2**	**3**	**4**	**5**	**6**
T (°C)	**Su**	$22,62 \pm 3,42$	$22,62 \pm 1,20$	$22,8 \pm 0,97$	$23,17 \pm 1,20$	$22,72 \pm 0,65$	$23,26 \pm 0,45$
	Au	$16,18 \pm 3,14$	$18,54 \pm 2,19$	$18,52 \pm 2,13$	$18,60 \pm 2,45$	$19,40 \pm 2,31$	$19,08 \pm 2,09$
	Wi	$14,78 \pm 2,07$	$15,41 \pm 0,44$	$15,56 \pm 0,44$	$15,73 \pm 0,42$	$15,91 \pm 0,78$	$16,03 \pm 16,03$
	Sp	$23,05 \pm 7,85$	$20,25 \pm 4,45$	$21,05 \pm 5,30$	$21,00 \pm 4,24$	$22,00 \pm 6,50$	$21,60 \pm 5,23$
SAL (%)	**Su**	$25,80 \pm 7,67$	$37,24 \pm 1,05$	$37,12 \pm 1,40$	$36,62 \pm 1,52$	$37,04 \pm 0,75$	$37,12 \pm 0,76$
	Au	$20,18 \pm 9,95$	$37,84 \pm 0,40$	$37,20 \pm 0,86$	$37,62 \pm 0,70$	$35,90 \pm 2,82$	$37,80 \pm 0,29$
	Wi	$20,55 \pm 8,07$	$37,48 \pm 0,71$	$37,48 \pm 0,57$	$37,66 \pm 0,27$	$37,91 \pm 0,70$	$37,83 \pm 0,67$
	Sp	$21,60 \pm 13,29$	$35,70 \pm 0,28$	$36,55 \pm 0,92$	$36,90 \pm 1,27$	$37,25 \pm 0,35$	$36,70 \pm 0,99$
pH	**Su**	$8,60 \pm 0,29$	$8,75 \pm 0,37$	$8,74 \pm 0,32$	$8,85 \pm 0,04$	$8,77 \pm 0,17$	$8,60 \pm 0,39$
	Au	$8,10 \pm 0,67$	$8,67 \pm 0,23$	$8,63 \pm 0,28$	$8,70 \pm 0,21$	$8,56 \pm 0,16$	$8,56 \pm 0,40$
	Wi	$8,60 \pm 0,28$	$8,51 \pm 0,18$	$8,60 \pm 0,16$	$8,62 \pm 0,15$	$8,58 \pm 0,12$	$8,58 \pm 0,17$
	Sp	$8,89 \pm 0,04$	$8,70 \pm 0,39$	$8,60 \pm 0,32$	$8,63 \pm 0,23$	$8,58 \pm 0,21$	$8,60 \pm 0,16$

Table 1: Water parameters (T (°C), Sal (%), pH) collected from Messina beachrock. Results are shown as mean value ± standard deviation.

3.2 Macrofaunal community

A total of 11635 specimens belonging to 34 different taxa were surveyed in Messina beachrock. They belong to six phyla as follows: Arthropoda (9), Chordata (6), Cnidaria (3), Echinodermata (7), Mollusca (8) and Porifera (1). Specimens belonging to the phylum Chordata (not relevant to our purposes) as well as those specimens considered occasional (*i.e.* found in less than three samples) were disregarded from statistic analysis, obtaining an amount of 11571 individuals (Table 2). Seasonal and spatial trends in the ecological descriptors A, S, J', H' are shown in Fig.4. Macrofaunal parameters showed a wide range of variability. Abundance ranged from 0.005 (ST1, Spring) to 16.654 (ST6, Winter) individuals/m^2. The highest number of species (16) was observed in station 6 in autumn, while the lowest (1) was observed in station 1 in spring. Pielou's evenness index (J') ranged from 1 (ST1, Spring) to 0.116 (ST6, Autumn). Shannon-Wiener's species diversity index (H') ranged from 0 (ST1, Spring) to 2.087 (ST3, Spring). Abundance (A) and specific richness (S) showed

spatial fluctuations between the stations (respectively $p = 0.003$ and $p = 0.002$). For both ecological descriptors, the Tukey test revealed significant differences between ST1 vs ST3 ($p = 0.002$) and ST1 vs ST6 ($p = 0.006$). The evenness (J') ($p = 0.005$) and Shannon-Wiener diversity (H') ($p = 0.023$) also showed significant spatial differences. Regarding J', relevant differences were observed between ST1 vs ST6 ($p = 0.002$) while, for H', the main differences were observed between ST3 and ST6 ($p = 0.031$).

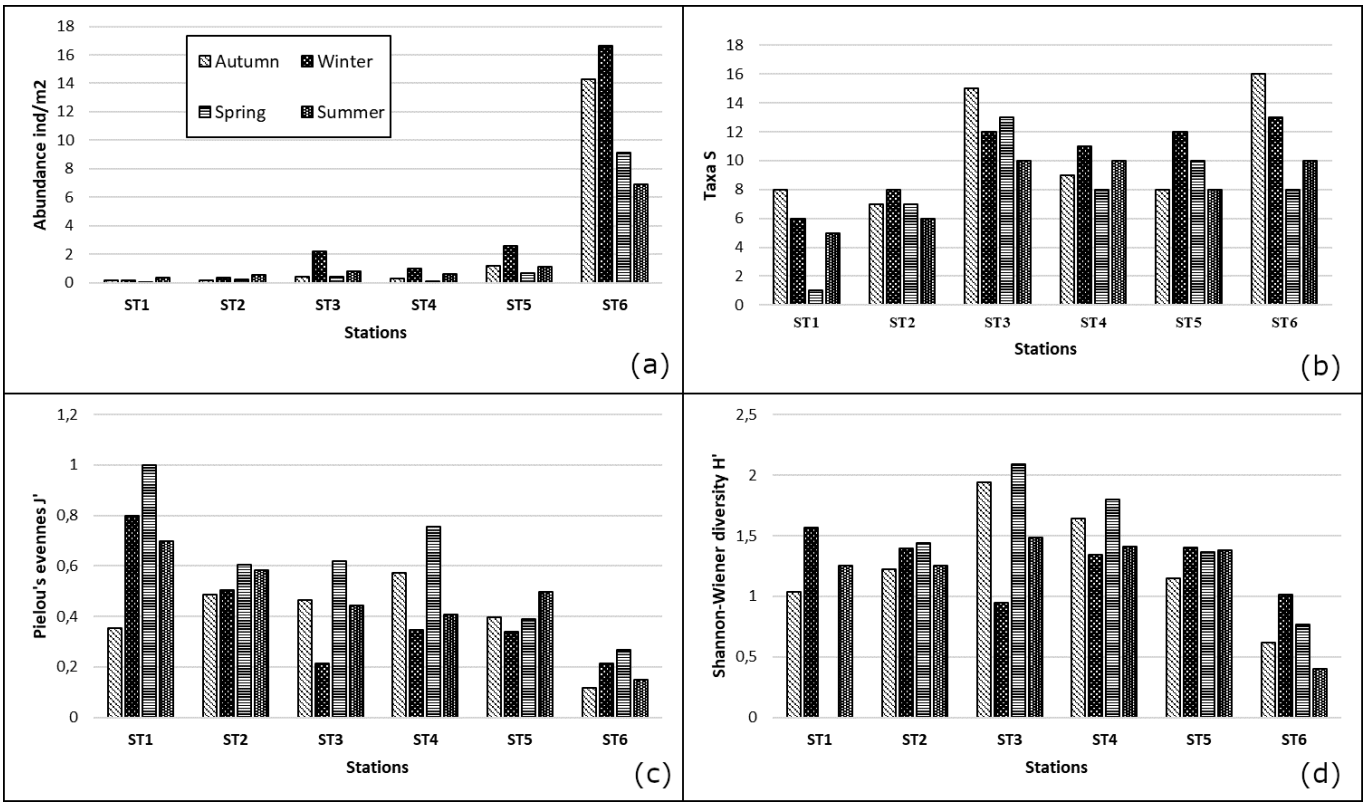

Figure 4: Spatial and seasonal trend of the main biological parameters in Messina beachrock: (a) Abundance; (b) Number of species, (c) Pielou's evenness and (d) Shannon-Wiener index.

3.3 Multivariate analysis

The BIO-ENV procedure showed a low degree of correlation between environmental and biological data. Salinity resulted the variable with the largest correlation coefficient, *i.e.* $\rho = 0.305$.

Cluster analysis and MDS ordination grouped the whole set of data, by season and station, into four main clusters (Fig.5). In detail, cluster I included the largest number of stations, with similar values of abundance and number of species. The most represented species were: *P. turbinatus*, *C. erythropus* and *P. cerulea*, with abundance values (in individuals/m^2) ranging from 0.003 to 0.229, from 0 to 0.347 and from 0 to 0.095 respectively. Cluster II included four seasonal samplings that exhibited analogue abundance values. The most representative species were *P. marmoratus* (0.004-0.017), *C. erythropus* (0-0.01) and *P. turbinatus* (0-0.002). Cluster III enclosed all the samples from Station 6, resulting characterized by the highest values of abundance for all surveyed species further than by the highest species richness. In particular, *A. sulcata* was the most abundant species (1.754-2.111), followed by *C. erythropus* (0.111-0.891) and *P. turbinatus* (0.003-0.562). At last, the single

Species	**Phylum**	**N. of specimens**
Actinia equina (Linnaeus, 1758)	Cnidaria	102
Anemonia sulcata (Pennant, 1777)	Cnidaria	6683
Aplysia dactylomela (Rang, 1828)	Mollusca	119
Aplysia fasciata (Poiret, 1789)	Mollusca	3
Arbacia lixula (Linnaeus, 1758)	Echinodermata	26
Arca noe (Linnaeus, 1758)	Mollusca	5
Halichondria (Fleming, 1828)	Porifera	21
Cerithium vulgatum (Bruguière, 1792)	Mollusca	93
Clibanarius erythropus (Latreille, 1818)	Arthropoda	2420
Coscinasterias tenuispina (Lamarck, 1816)	Echinodermata	16
Echinaster sepositus (Retzius, 1783)	Echinodermata	14
Eriphia verrucosa (Fosrkal, 1775)	Arthropoda	19
Hexaplex trunculus (Linnaeus, 1758)	Mollusca	41
Holoturia sanctori (Delle Chiaje, 1823)	Echinodermata	3
Holoturia tubulosa (Gmelin, 1791)	Echinodermata	19
Maja crispata (Risso, 1827)	Arthropoda	3
Pachygrapsus marmoratus (Fabricius, 1787)	Arthropoda	159
Dardanus arrosor (Herbst, 1796)	Arthropoda	5
Palaemon elegans (Rathke, 1837)	Arthropoda	18
Paracentrodus lividus (Lamarck, 1816)	Echinodermata	8
Patella caerulea (Linnaeus, 1758)	Mollusca	343
Percnon gibbesi (H. Milne Edwards, 1853)	Arthropoda	3
Phorcus turbinatus (Born, 1778)	Mollusca	1444
Xanto poressa (Olivi, 1792)	Arthropoda	4

Table 2: List of the species.

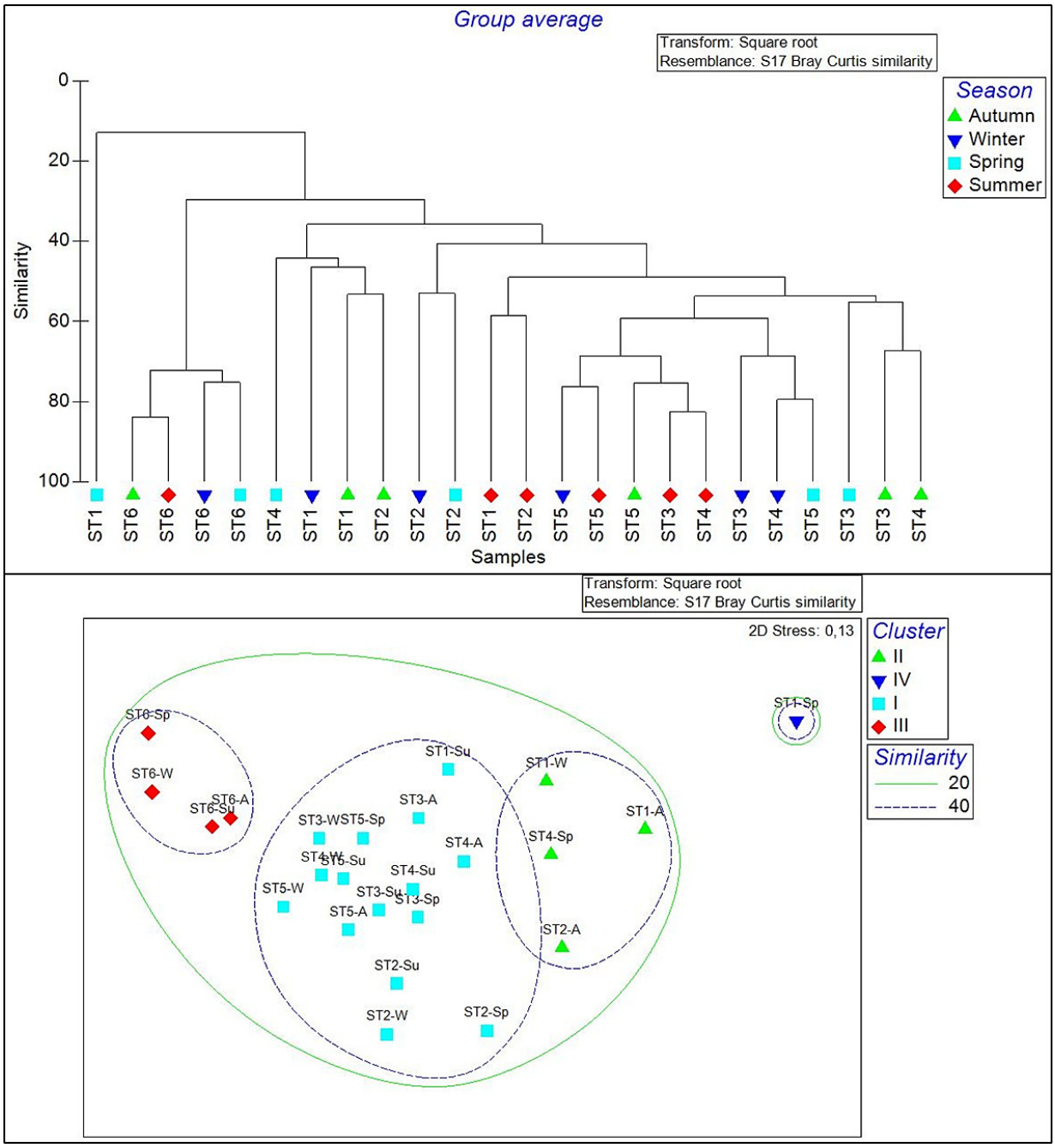

Figure 5: Dendrogram and MDS ordination of Bray-Curtis similarities from abundance data (square root transformation) for 6 sampling stations in the intertidal zone of Messina beachrock. (A=Autumn; W=Winter; Sp=Spring; Su=Summer).

ST1-Sp (cluster IV) was the only station where *C. erythropus* and *P. turbinatus* were absent, apart from being the station characterized by the lowest number of specimens.

The outcome of SIMPER analysis, reported in Table 3, revealed that the most significant similarity between group members was associated to cluster III (average similarity: 74.68), followed by the cluster I (average similarity: 52.69). Table 3 also includes the percentage contribution of the main species to the similarity within each group. Regarding cluster I, the species with the highest contribution were *P. turbinatus*, *C. erythropus* and *P. cerulea*, with a percentage of 25.55%, 25.27% and 17.71%, respectively. In cluster II, the highest contribution was given by *P. marmoratus*, as numerically more abundant, followed by *C. erythropus* and *P. turbinatus* with percentages of 43.37%, 17.1% and 11.05%, respectively. At last, for cluster III, *A. sulcata* was the most abundant species, with a percentage of 62.54%, while *C. erythropus* and *P. turbinatus* amounted to 18.81% and 6.62%, respectively.

Therefore, *P. cerulea*, *P. marmoratus* and *A. sulcata* resulted numerically significant even though each of the above species contributed in just one cluster (I, II and III, respectively). On the contrary, *C. erythropus* and *P. turbinatus* provided a relevant contribution in all of the above clusters and, resulting in a wider spatial and seasonal distribution, may be considered as the most characteristic beachrock species.

Although non-statistically significant, *Cerithium vulgatum* (Bruguière, 1792) is another species of interest in this work. This species showed a singular and isolated abundance event that may be put in relation to the trend exhibited by *P. turbinatus* and *C. erythropus*. In fact, for all analyzed clusters, in the period between winter and spring, a decrease of *P. turbinatus* specimens was accompanied by a concurrent increase of both *C. vulgatum* and *C. erythropus*. These results suggested us to inspect further on possible interactions among these species. This analysis is addressed in the next section.

3.4 Assessing prey-predator dynamics

Results of multivariate analysis indicate that two most representative species inhabiting Messina beachrock pools are the hermit crab *C. erythropus* and the top-snail *P. turbinatus* (see Fig.6). A marginal role is played by the sediment feeder *C. vulgatum*, due to its limited availability over the whole observation period. In this food web, *C. erythropus* plays the role of a shared predator being a second-order consumer which preys both *P. turbinatus* and *C. vulgatum* [41].

To assess prey-predator interactions among these species, we now inspect in detail the results of the visual census procedure carried out over a period of 15 months (from 18 October 2016 to 17 January 2018). Results depicted in Fig.7 allow to clearly elucidate the respective roles of the species here involved and to identify four different dynamical regimes, that are now analyzed separately.

3.4.1 Predator-free state

During the whole sampling period, we reported two single events characterized by the absence of predators. Interestingly, this scenario took place with a periodicity of one year, in late November 2016 and early December 2017, although the amount of *P. turbinatus* prey species was notably different, counting 67 and 258 specimens, respectively. No events with the presence of *C. vulgatum* alone were noticed.

Cluster I					
	Average similarity: 52.69				
Species	**Av.Abund**	**Av.Sim**	**Sim/SD**	**Contrib%**	**Cum.%**
P. turbinatus	0.22	13.99	2.22	25.55	26.55
C. erythropus	0.24	13.32	1.67	25.27	51.82
P. caerulea	0.14	0.33	1.66	17.71	69.53
P. marmoratus	0.08	4.45	1.14	8.44	77.97
A. dactylomela	0.07	3.45	0.89	6.55	84.52
A. equina	0.05	1.98	0.76	3.75	88.27
H. trunculus	0.03	1.61	0.83	3.06	91.34
Cluster II					
	Average similarity: 46.43				
Species	**Av.Abund**	**Av.Sim**	**Sim/SD**	**Contrib%**	**Cum.%**
P. marmoratus	0.10	20.14	4.50	43.37	43.37
C. erythropus	0.05	7.94	3.21	17.10	60.47
P. turbinatus	0.04	5.13	0.89	11.05	71.52
H. trunculus	0.03	4.71	0.90	10.15	81.67
P. caerulea	0.05	3.90	0.89	8.40	90.07
Cluster III					
	Average similarity: 74.68				
Species	**Av.Abund**	**Av.Sim**	**Sim/SD**	**Contrib%**	**Cum.%**
A. sulcata	1.41	46.71	11.25	62.54	62.54
C. erythropus	0.62	14.05	2.47	18.81	81.36
P. turbinatus	0.33	4.94	1.43	6.62	87.98
A. equina	0.10	2.31	3.45	3.09	91.07

Table 3: The most representative species that contributed to the similarity within each cluster, determined by SIMPER analysis.

Figure 6: (left and center) Living *P. turbinatus* and (right) shell occupied by *C. erythropus* after predation. (Photo by Marco Albano)

3.4.2 Recruitment peaks

Both *P. turbinatus* and *C. erythropus* underwent two recruitment peaks per year (see Fig.7(b)). The first event took place in late February, as a sudden increase in both species amount, with 5 days delay of predator population in respect to preys. Once the prey recruitment has finished, a new predator settlement originated in early April, although without a preceding population increase of *P. turbinatus*, that remained almost constant. Interestingly, the second predator "bloom" started with an almost simultaneous increase of its alternative prey, *C. vulgatum*, as it can be noticed in Fig.7(a). The population size of this latter species remained negligible throughout the remaining sampling period.

Another recruitment peak of the prey *P. turbinatus* occurred in late October 2017, but it was not coupled with a predator population increase.

3.4.3 Co-existence state

It is interesting to notice that, before and after the two predator "blooms", populations of *P. turbinatus* and *C. erythropus* did not undergo significant fluctuations, approximately maintaining their equilibrium values over a period of about one month. An analogous equilibrium period of about 20 days was observed before the occurrence of the second *P. turbinatus*'s recruitment peak.

3.4.4 Periodic behavior

An intriguing dynamics took place in the period ranging from 20 June to 20 July 2017, when the populations of *P. turbinatus* and *C. erythropus* oscillated periodically around their equilibrium values, as proven by superimposing a sinusoidal fit on the collected data (see Fig.7(c)). The resulting agreement also revealed a constant phase shift (about 2 days) in the time evolution of the two populations.

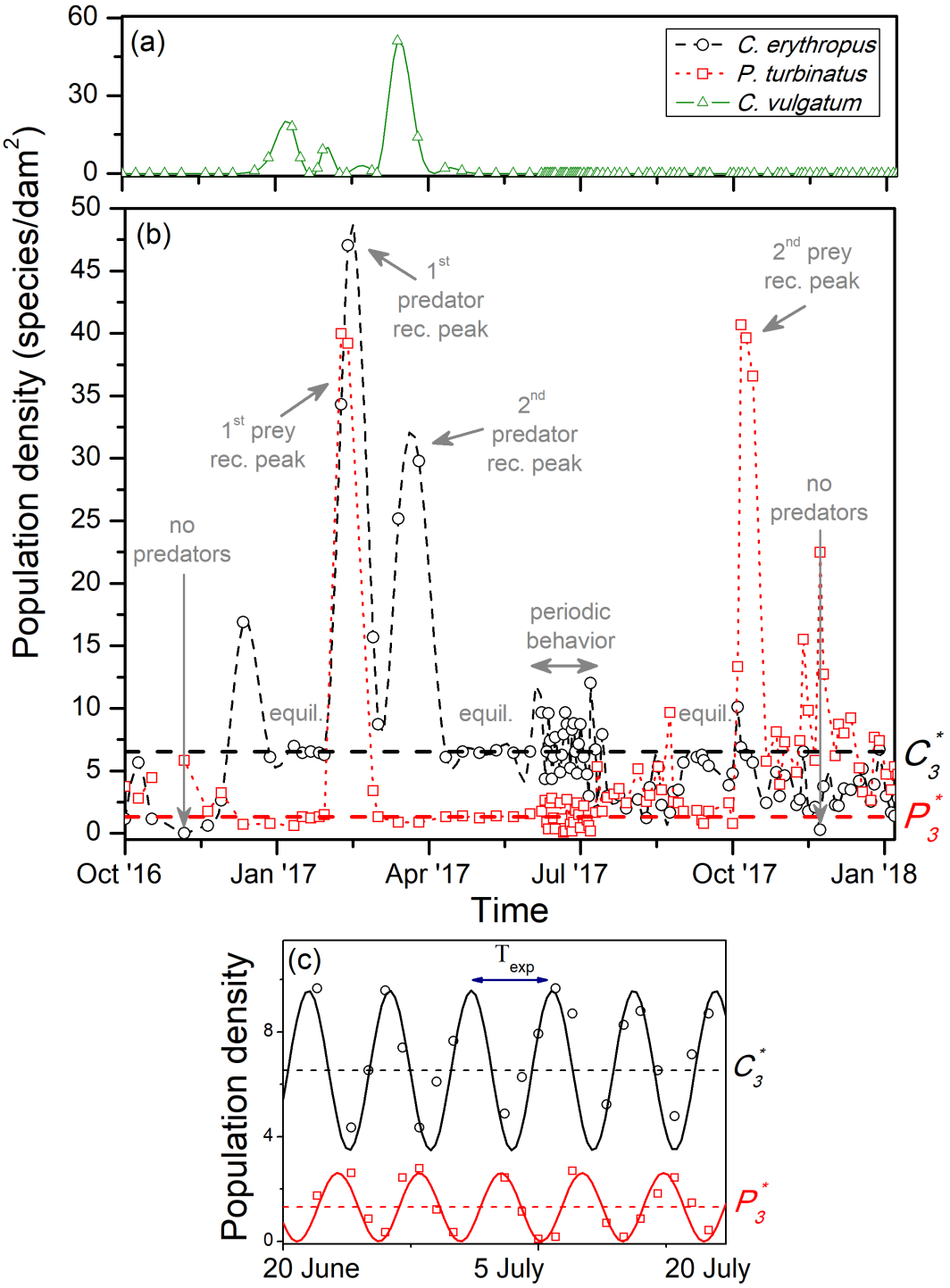

Figure 7: (a,b) Time evolution of the densities of *C. erythropus* (black circles), *P. turbinatus* (red squares) and *C. vulgatum* (green triangles) over a 15-months period resulting from *in situ* measurements. Horizontal dashed lines denote the equilibrium populations reported in (4, 5) whereas vertical arrows represent predator-free states. The total number of species is normalized with respect to the overall surface covered by the six stations ($S = 1147.87$ m^2). (c) A detail of the periodic behavior observed between 20 June and 20 July 2017. Here, symbols are the same as in (b), whereas continuous lines are the result of least square sinusoidal fitting of the collected data with a period $T_{exp} = 4.8$ days.

3.5 Mathematical description of prey-predator interactions and parameters identification

In this Section we investigate whether the mathematical model presented in Section 2.5 could provide a qualitative description for the different dynamical regimes observed *in situ*. In particular, we inspect which model parameters play an active role in each stage and carry out their numerical identification accordingly.

To this aim, in the proposed model (1), we associate $P(t)$ and $C(t)$ with the time evolution of the population densities of *P. turbinatus* and *C. erythropus*, respectively.

Notice that, the *C. vulgatum* population density is not taken as an additional state variable owing to its negligible abundance over the whole sampling period together with its time-limited role in the trophic chain. However, we assume that the occasional presence of this alternative prey enters the model as an external factor affecting predator's mortality rate m.

3.5.1 Predator-free state

These ecological scenarios may be put in relation with the occurrence of the state $E_2^* = (k, 0)$ that becomes stable, and thus observable in the studied environment, if the predator mortality is larger than the critical value ($m > m_{cr}$). In these cases, the amount of preys detected in the tidal ponds may provide a direct estimation of the carrying capacity. According to our observations, it fluctuated from $k = 67/S = 5.84$ species/dam^2 (at November 2016) to $k = 258/S = 22.48$ species/dam^2 (at December 2017). Therefore, the carrying capacity of such intertidal rocky pools may undergo large fluctuations over time.

3.5.2 Recruitment peak

We can hypothesize that, during the simultaneous bloom of both species, the carrying capacity has even achieved much larger values than those previously estimated. Indeed, according to model (1), the increase of the carrying capacity represents the only possibility for both populations to achieve such large sizes. About the bloom of the only predators, we infer that this phenomenon might be related to reproductive events [42, 43]. However, the second predator bloom might coincide with a pre-reproductive phase of *C. erythropus*. Furthermore, in this case, we can suppose that the hermit crab's bloom can be linked to the contemporary availability of some alternative preys to *P. turbinatus*. In particular, during this phase, a significant abundance of *C. vulgatum* was recorded (see Fig.7(a)), which should have guaranteed the ideal trophic conditions to the predator (high carrying capacity and low mortality).

Instead, the second prey's bloom, observed at the end of October 2017, might be justified by a simultaneous increase of carrying capacity (for instance, due to a larger availability of trophic resources) and a simultaneous scarcity of predators (for instance, due to a temporary high predator's mortality rate).

3.5.3 Co-existence state

The one month-periods in which both prey and predators remained at their equilibrium values are representative of a stable co-existence state $E_3^* = (P_3^*, C_3^*)$. In Fig.7(b), such constant stages are depicted by dashed horizontal lines. It is also remarkable that the sizes of the two populations

detected at equilibrium were approximately the same, independently of the season in which they have been reported ($P_3^* = 1.3$ species/dam^2, $C_3^* = 6.5$ species/dam^2).

From the mathematical viewpoint, by using (4),(5), we deduce the following constraints on the model parameters μ, β and λ:

$$\mu\sqrt{\frac{m}{\lambda - m}} = 1.3 \text{ species/dam}^2, \tag{15}$$

$$\frac{\beta}{m}\left(1 - \frac{1.3}{k}\right) = 5. \tag{16}$$

Owing to the stability of this steady state, we also infer that, in the above-mentioned periods, the predator mortality is smaller than the critical value ($m < m_{cr}$) whereas the carrying capacity has to satisfy the constraints given in (11).

3.5.4 Periodic behavior

The observed periodic behavior may be strictly related to the occurrence of a Hopf bifurcation. From the theoretical viewpoint, from (10),(12) we get an additional constraint among the parameters k, m and λ:

$$k = \frac{2m}{2m - \lambda}P_3^*. \tag{17}$$

Moreover, the efficiency parameter ϵ can be estimated from the field observation that the period of oscillation is $T_{\text{exp}} = 4.8$ days (as denoted in the inset of Fig.7(c)). Considering the non-negligible amplitude of these oscillations, it is reasonable to assume that they took place far from threshold. For this reason, from expression (14) we set:

$$2\pi\left[\frac{2\epsilon\beta m\,(\lambda - m)}{\lambda}\left(1 - \frac{\mu}{k}\sqrt{\frac{m}{\lambda - m}}\right)\right]^{-1/2} = 4 \text{ days}. \tag{18}$$

3.5.5 Parameter estimation results

The above analyses provided confirmation that the model (1) may be used to qualitatively mimic the intriguing dynamics occurring in Messina's beachrock pools. As a consequence of that, we can use the above information to estimate all the model parameters.

Therefore, by setting the carrying capacity at the value $k = 5.84$ species/dam^2 (as deduced from the data reported at November 2016), the parameters μ, λ, β and ϵ can be determined as follows:

$$\begin{aligned} \mu &= 0.97 \text{ species/dam}^2, \\ \lambda &= 1.55m \text{ days}^{-1}, \\ \beta &= 6.44m \text{ days}^{-1}, \\ \epsilon &= \tfrac{0.6935}{m^2}. \end{aligned} \tag{19}$$

Let us notice that, because of the ecological meaning of the efficiency parameter $\epsilon < 1$, the condition $(19)_4$ sets a lower bound on the allowed mortality rate m. The above constraints are graphically represented in Fig.8.

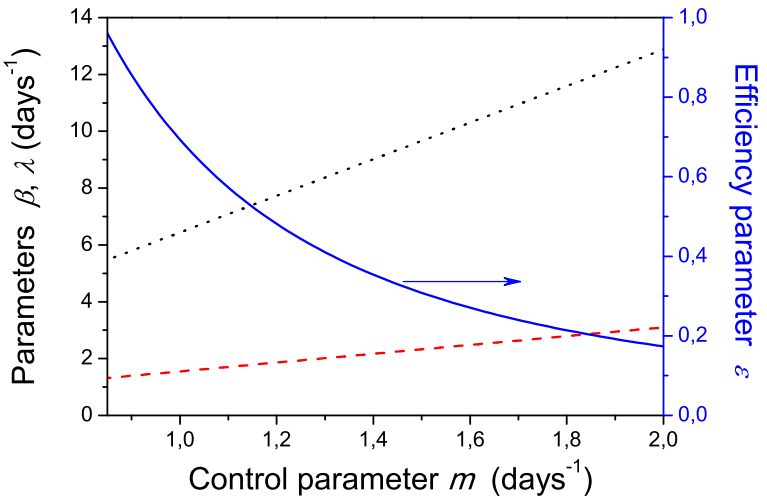

Figure 8: Dependence of the model parameters β (dotted black line), λ (dashed red line) and ϵ (solid blue line) as a function of the mortality-related parameter m.

For instance, by setting the conversion efficiency at $\epsilon = 0.2$, we get: $m = 1.86$ days^{-1}, $\beta = 12$ days^{-1}, $\lambda = 2.88$ days^{-1}, $m_{cr} = 2.80$ days^{-1}, $k_{min} = 5.04$ species/dam^2. It is easy to verify that this parameter set verifies the conditions $m < m_{cr}$ and $k > k_{min}$ required for the occurrence of Hopf bifurcation.

3.6 Numerical simulations

We aim at exploring the different ecological dynamics arising from the above model and, in particular, at mimicking the dynamics observed *in situ* (see Fig.7(b)) through the use of the parameter values previously identified.

The common parameters used in the simulations are: $\mu = 0.97$ species/dam^2, $\beta = 6.44$ days^{-1}, $\epsilon = 0.6935$, $\lambda = 1.55$ days^{-1} and $k = 5.84$ species/dam^2. The initial conditions are specified in the captions of the figures.

Let us now investigate, first, dynamics corresponding to the evolution towards a stable equilibrium. In Fig.9(a,b) we depict the behavior obtained when the condition $m > m_{cr}$ is met. As it can be seen, the system converges toward the stable predator-free state E_2^*. Since this scenario has been observed two times during the whole sampling period, in both cases in the form of an isolated event, we believe that the relatively large value of predator mortality occurred for a very reduced time.

In Fig.9(c,d) and (e,f) we consider the setup corresponding to $m < m_{cr}$, so that the predator-free state E_2^* is unstable whereas the co-existence state E_3^* is stable. This latter condition is ensured by the requirement $m < m_1^H$, so that the system does not lie in the instability interval. As it can be seen, after a transient in which the population exhibits an overshoot with respect to the equilibrium density, the system converges toward E_3^* but in a different manner. In (c,d), it relaxes exponentially, whereas in (e,f) it exhibits damped oscillations. This can be justified because the characteristic polynomial (6) admits real eigenvalues in the former case whilst complex conjugate eigenvalues in the latter case. We believe that, most likely, such dynamics may have been occurred when the population densities were close to their equilibrium values.

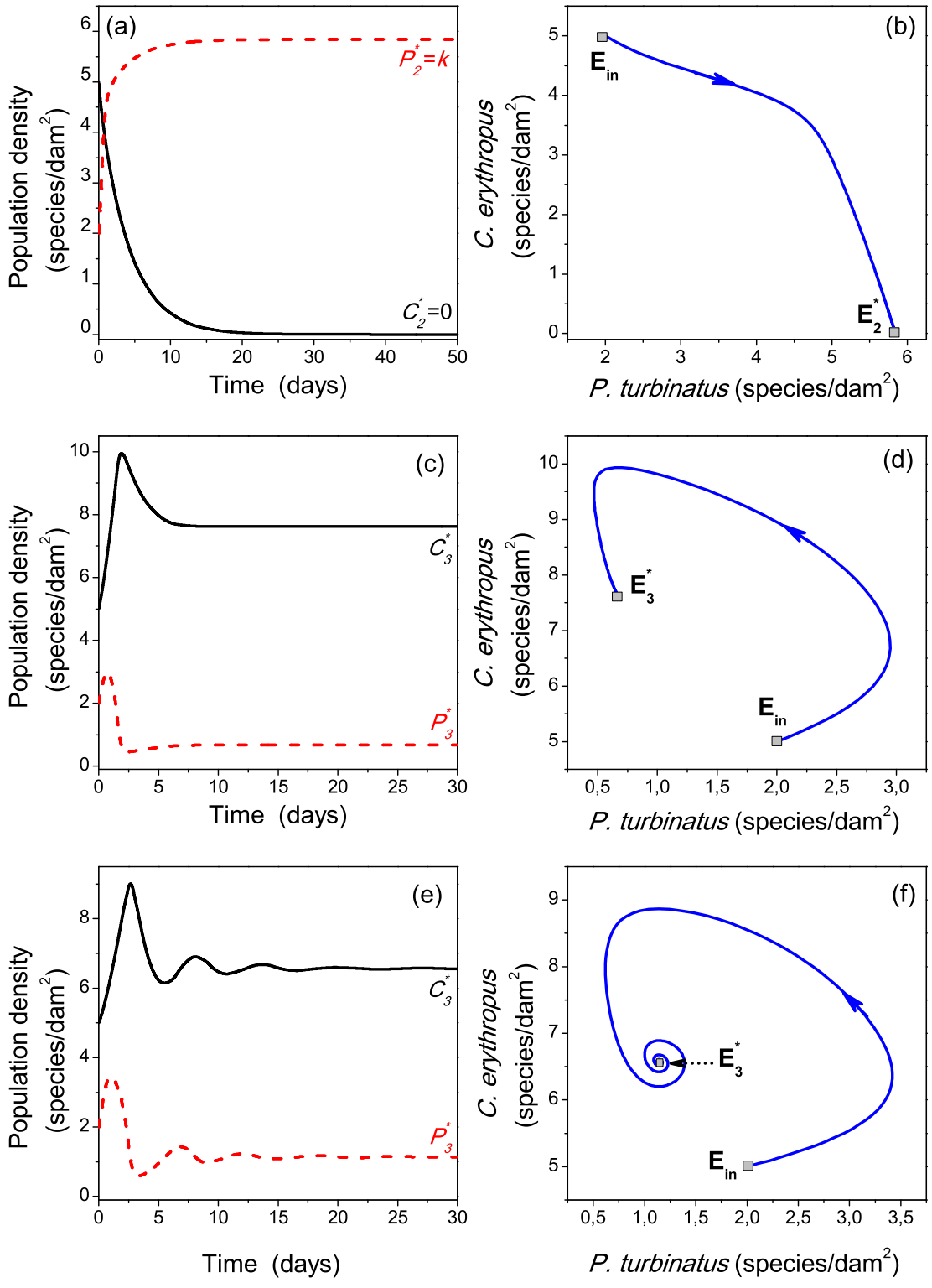

Figure 9: Evolution towards stable equilibrium. (a,c,e) Time evolution of predators (solid black line) and preys (dashed red lines); (b,d,f) the corresponding phase-plane diagrams. The common parameters used in the simulations are: $\mu = 0.97$ species/dam^2, $\beta = 6.44$ days^{-1}, $\epsilon = 0.6935$, $\lambda = 1.55$ days^{-1} and $k = 5.84$ species/dam^2. The other parameters are: (a,b) $m = 2$ days^{-1}; (c,d) $m = 0.5$ days^{-1}; (e,f) $m = 0.9$ days^{-1}. The initial condition is $E_{in} = (P_{in}, C_{in}) = (2, 5)$ species/dam^2.

Let us now investigate numerically the scenario in which both species undergo a periodic oscillation around their equilibrium values. To this aim, we assume that the mortality parameter takes a value $m_1^H < m < m_2^H$, so that the co-existence state loses its stability via a Hopf bifurcation. Results are depicted in Fig.10. It is interesting to notice that the value of the mortality rate here considered ($m = 1.11$ days^{-1}) is just 20% larger than the one used in Fig.9 ($m = 0.9$ days^{-1}) that leads the system to relax toward the equilibrium state. In order words, by leaving all the other parameters unchanged, a slight increase of the predator mortality suffices to generate such periodic oscillations. Figs.10(b,d) show the evolution of the system in the (P, C) phase-plane and reveal the existence of a stable limit cycle. Indeed, by choosing initial conditions that falls outside (as in (b)) or inside (as in (d)), the system converges to the limit cycle. It is also interesting to notice that the numerically computed value of the period of oscillation, T_{num}=4.7 days, agrees quite well with the one extracted from sampling data, T_{exp}=4.8 days.

Finally, we try to mimic numerically the dynamics and the time scales characterizing the different, and complex, bloom phases. To this aim, in accordance with the hypotheses made in section 3.5.2, we consider dynamics that originates from the equilibrium state and deviate away from it as a consequence of smooth periodic and/or aperiodic perturbations of carrying capacity and predator's mortality [31, 32], as illustrated in Figs.11-13(a,b). We implement a one-year event for the mortality rate $m(t)$ (from day 240 to 300) and a twice-a-year event for the carrying capacity $k(t)$ (from day 0 to 50 and from day 240 to 300, respectively), based on *in situ* data. Moreover, to account for the singular and isolated abundance of *C. vulgatum*, an aperiodic disturbance leading to a decrease of predator's mortality is added in a limited time window (from day 25 to 50).

This setup allows us to reproduce qualitatively the three recruitment peaks. Indeed, the increase of the carrying capacity at day 20 destabilizes the system and lets both populations to grow significantly, with predators exhibiting a small delay with respect to preys. After having achieved a maximum, both species return close to their equilibrium values (day 30). Then, the occurrence of a downward shift of predator's mortality causes the initiation of the recruitment stage for the only predator population. Prey population initially follows predator's growth but the amount of predators is now so significant that preys are quickly killed and return to their equilibrium value. Then, when both control parameters return to their initial values, the system evolves toward the stable co-existence state (day 50). This behaviour is consistent with the data sampled in the period from February to April 2017. At approximately day 240, the simultaneous increase of carrying capacity and mortality leads to a second prey's bloom not followed by an analogous predator's one, in agreement with the behaviour observed in October 2017. These dynamics are summarized in Fig.11(c).

Moreover, in order to establish periodic oscillations of both populations, we superimpose an aperiodic disturbance to predator's mortality from day 140 to 210, as shown in Fig.11(a). As it can be noticed, an increase of about 20% in the mortality parameter m generates a periodic behaviour in both populations from day 170 to 200 (see Fig.11(c)), which is compatible with the oscillations reported in the period ranging from 20 June to 20 July (see Fig.7(c)).

Finally, in order to evaluate whether such periodic oscillations may be destroyed by time-varying control parameters, we consider two additional scenarios where the function $k(t)$ is perturbed via an additive periodic or random disturbance over a wider temporal window (from day 100 to 220). To account for non-negligible variations of carrying capacity, the amplitude of these perturbations is about 50% of the stationary value. Results illustrated in Figs.12,13(c) reveal that the periodic behavior still survives in the presence of the considered fluctuations.

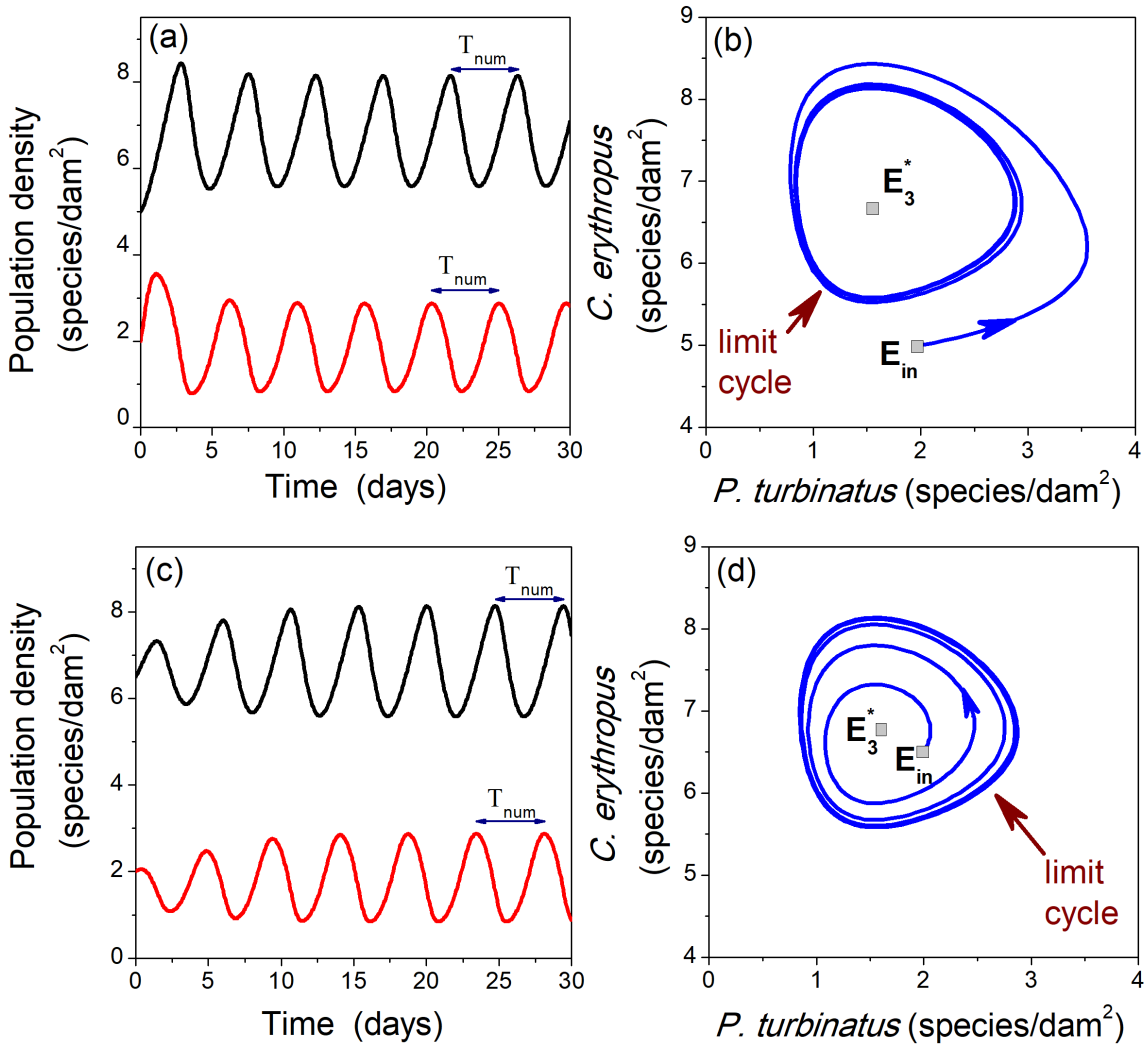

Figure 10: Periodic behavior. (a,c) Time evolution of predators (solid black line) and preys (dashed red lines); (b,d) the corresponding phase-plane diagrams. The common parameters used in the simulations are: $\mu = 0.97$ species/dam^2, $\beta = 6.44$ days^{-1}, $\epsilon = 0.6935$, $\lambda = 1.55$ days^{-1}, $k = 5.84$ species/dam^2 and $m = 1.11$ days^{-1}. The initial conditions are: (a,b) $E_{in} = (2, 5)$ species/dam^2; (c,d) $E_{in} = (2, 6.5)$ species/dam^2. The numerically-computed period of oscillations is $\mathrm{T_{num}} = 4.7$ days $\simeq \mathrm{T_{exp}}$.

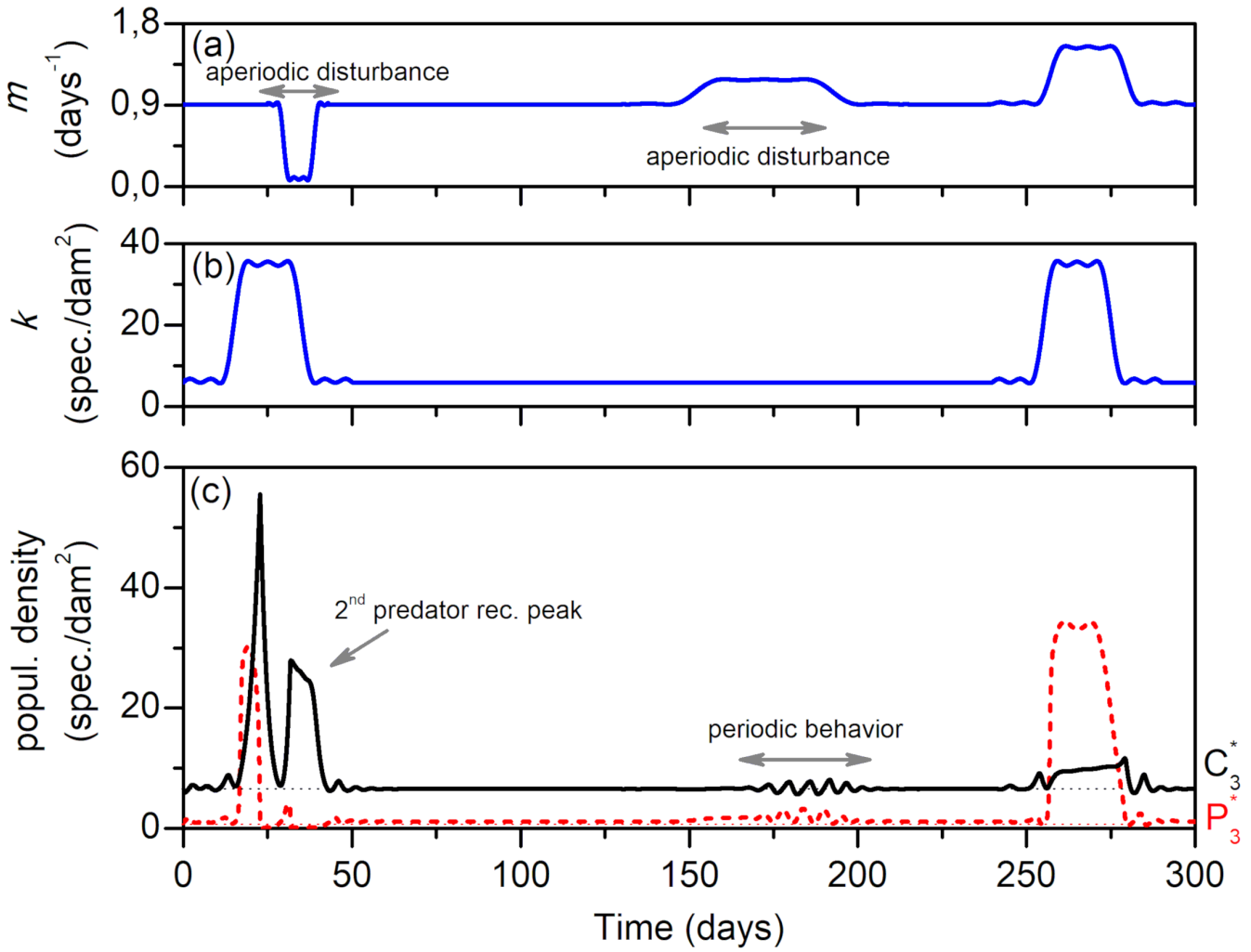

Figure 11: (a,b) Time evolution of parameters k and m employed to qualitatively mimic the dynamics observed *in situ*. The other parameters are: $\mu = 0.97$ species/dam^2, $\beta = 6.44$ days^{-1}, $\epsilon = 0.6935$ and $\lambda = 1.55$ days^{-1}. (c) Time evolution of prey and predator populations obtained by integrating numerically the system (1).

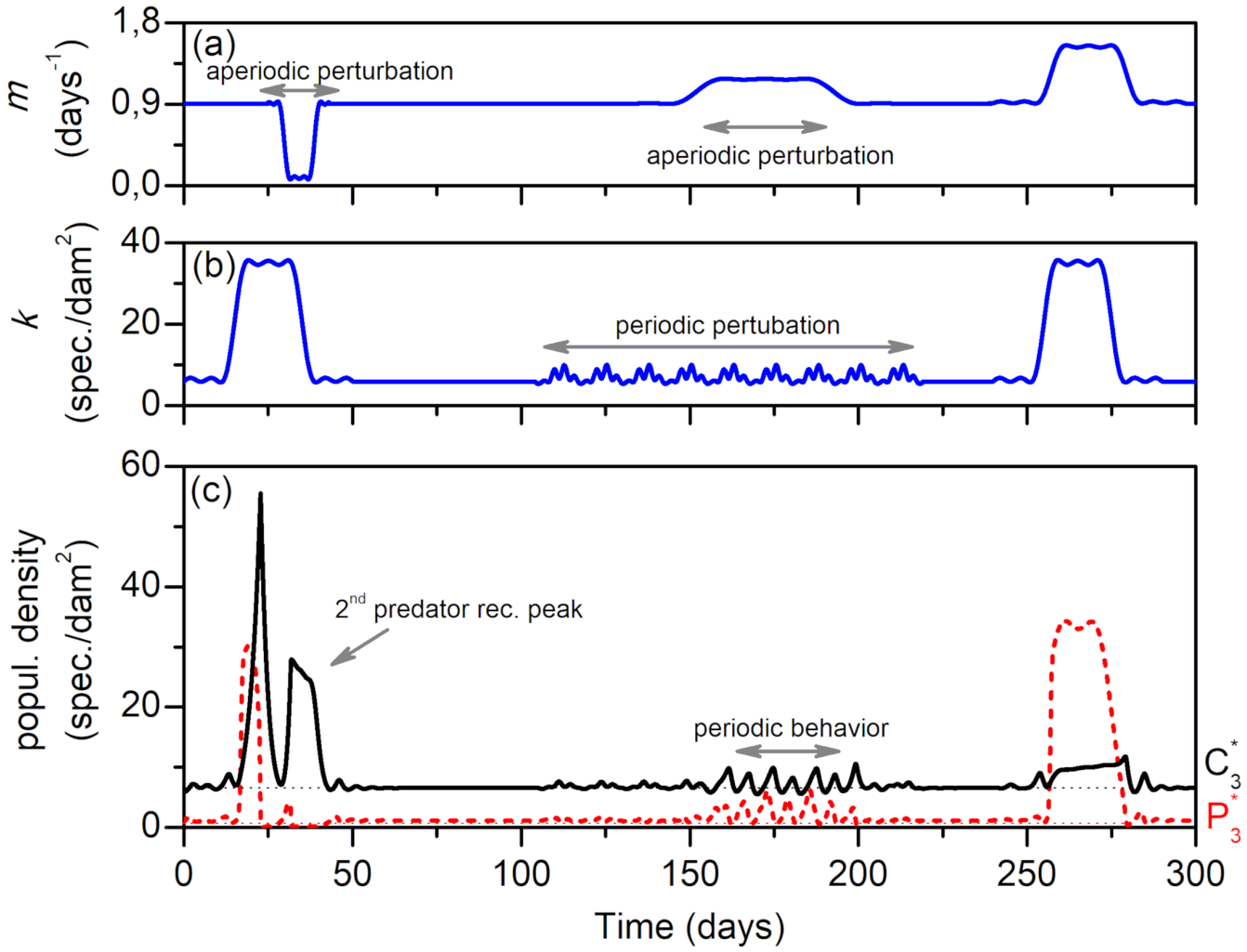

Figure 12: (a,b) Time evolution of parameters k and m employed to qualitatively mimic the dynamics observed *in situ*. The other parameters are: $\mu = 0.97$ species/dam^2, $\beta = 6.44$ days^{-1}, $\epsilon = 0.6935$ and $\lambda = 1.55$ days^{-1}. A periodic perturbation is superimposed to the carrying capacity from day 100 to 220. (c) Time evolution of prey and predator populations obtained by integrating numerically the system (1).

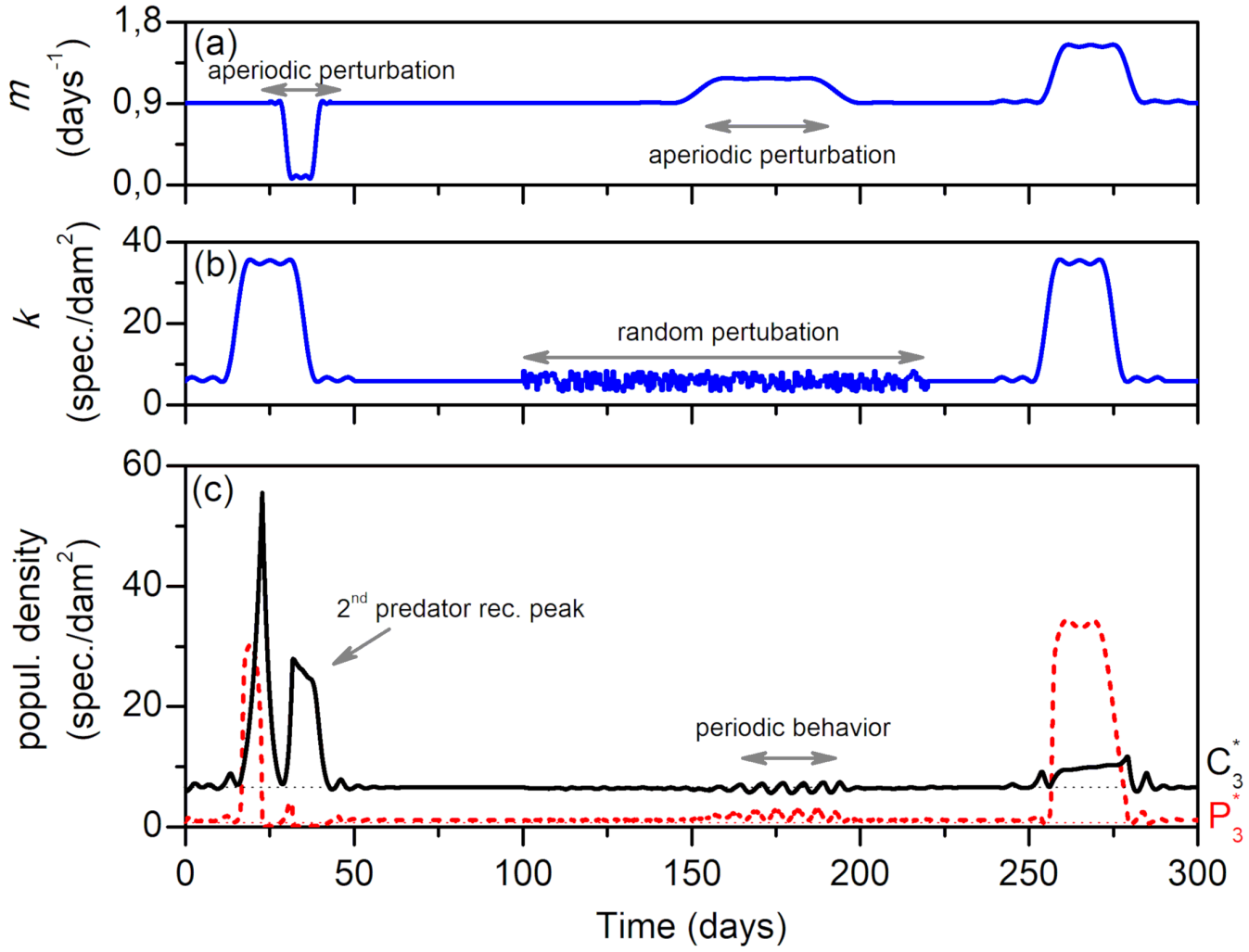

Figure 13: (a,b) Time evolution of parameters k and m employed to qualitatively mimic the dynamics observed *in situ*. The other parameters are: $\mu = 0.97$ species/dam^2, $\beta = 6.44$ days^{-1}, $\epsilon = 0.6935$ and $\lambda = 1.55$ days^{-1}. A random perturbation is superimposed to the carrying capacity from day 100 to 220. (c) Time evolution of prey and predator populations obtained by integrating numerically the system (1).

4 Discussion

Although beachrock formations are known from several Mediterranean coasts, the related benthic assemblages have been poorly investigated. Such environments, similarly to other shallower rocky formations [44], is subject to strong environmental (e.g. waves, drying, rain) and anthropogenic stressors (e.g. trampling), allowing the settlement of strictly oligotypic communities.

The Messina beachrock, scarcely affected by the local microtidal regime but exposed to seasonal sea-storms, hosts low diversity assemblages that, according to the SIMPER analysis, are characterized by a mixture of preferential intertidal (*Phorcus turbinatus*, *Patella caerulea*, *Pachygrapsus marmoratus*) and exclusive subtidal (*Anemonia sulcata*) elements, whose significant correlation with salinity underlines their euryhaline character.

Results of our investigations on beachrock pools revealed a homogeneous macro-benthic composition and distribution of the identified species from both spatial and seasonal viewpoints. Our results highlighted that the highest values of abundance, species richness and biodiversity are associated to station 6. Significant differences were detected between station 1 and station 6, as evidenced by the corresponding ecological descriptors ($p < 0.05$) and in particular between autumn and spring. Considering the similar physical and edaphic characteristics of these stations, we can hypothesize that the observed differences between these two areas may be determined by the different grade of water exchanges with the sea, as already reported in [20]. Station 1 is indeed characterized by very low seawater exchange, differently from the stations 6 which has a continuous exchange, allowing the movement of organisms from and towards the nearby marine areas.

Cluster analysis highlighted similarities in the composition of the macrobenthic community, for each station and season, in agreement with previous literature works [45, 46]. The most relevant differences were detected mostly in terms of abundance and species. As far as spatial variability is concerned, the Station 1 showed the smallest number of specimens, as well as the lowest number of species, particularly in the spring period. For these reasons, data belonging to ST1-Sp fell into cluster IV. On the other hand, data collected in Station 6 reported the largest number of specimens for each species here identified. We attributed such a large value of abundance to the physical, edaphic and hydrodynamics characteristics of this station [20]. Therefore, all seasonal samplings associated to Station 6 formed the single cluster III. Homogeneous results, in terms of abundance, especially for the *Hexaplex trunculus* species, were obtained in the ST1-A, ST1-W and ST2-A, ST4-Sp samples, which were grouped together in cluster II. Finally, cluster I enclosed the largest number of stations, that exhibited much more similar values of richness in species and abundance.

Additional information on the identified species, seasonal trend as well as on the features of stations were extracted via SIMPER analysis. In detail, the most representative species were *A. sulcata*, *C. erythropus*, *P. caerulea*, *P. marmoratus* and *P. turbinatus*, that are those species much more tolerant to a large variability of salinity (as reported in Table 1). In fact, as demonstrated by the BIOENV analysis, there was a significant correlation between salinity and identified species [47, 48, 49].

Data collected over a period of more than one year indicated a substantial stability and spatial homogeneity of such assemblages, as reported from other extreme environments [50, 51]. Local diversification shown by some ecological descriptors between St.1 and St.6, although statistically significant, does not involve a different ecological connotation, since probably tied to the different exposure and connection grade with the open sea. Indeed, our subdivision of the beachrock area into six stations is not representative of isolated and disconnected patches. The six randomly-

selected stations are, in fact, in close proximity with each other and are characterized by continuous exchange of both seawater and organisms (prey and predators) from and towards the nearby stations. Our disaggregated data revealed, in fact, that the population dynamics previously discussed occur simultaneously in all stations. As a result, the whole environment can be safely approximated through a spatially-uniform system with populations evolving with time.

Seasonal variability is high, but essentially stressed by the population dynamics of the two dominant vagile species, *P. turbinatus* and *C. erythropus*. These species provided indeed a significant contribution and showed the highest values of abundance in each station, but also exhibited a seasonal variability whose trends suggested a possible correlation between them. In particular, the increasing number of *P. turbinatus* specimens during winter and summer, alternated by a decrease in autumn and spring, agrees with the life cycle of this species which spawns during autumn and spring, so that an increase of abundance is expected in coincidence of the periods following the reproduction stage [52, 53]. On the other hand, *C. erythropus* exhibited a recruitment peak in all stations during winter, but also some other different localized growths in spring (Stations 5 and 6) and summer (Stations 1, 2, 3 and 4). In this respect, different dynamical regimes undergone by these two species were distinguished, such as the simultaneous presence of both species (lying at equilibrium for a given period), the predator-free state, an oscillating behavior and different bloom stages.

Previously-conjectured prey-predator relationship between *C. erythropus* (predator) and *P. turbinatus* (prey) was here definitively proved to hold [20]. To this aim, we proposed a mathematical model able to capture, at least qualitatively, the most intriguing dynamics observed in these two levels of the local trophic chain. It is interesting to mention that the model (1) is also used with success in other contexts. For instance, it may describe the prey-predator interactions occurring between phytoplankton and zooplankton [54, 55, 56].

In such marine trophic chains, the quantity of prey consumed per predator to prey density $h(P)$, is typically assumed to follow a Holling type-I, II or III FR [30]. Since a response of type-I is quite rare for predators that actively search for their preys [57], here we limit our discussion on type-II and III and provide those ecological and mathematical grounds in support of the assumptions made in this work.

From the *ecological* viewpoint, it is known that a Holling type-III FR is typically encountered in predators spending more time for hunting (searching) preys rather than for handling preys themselves [57]. In this case, the most used anti-predator tactics followed by preys to reduce the encounter rate with predators are: avoidance, residence in low-density patches, refuges and habitat structures (*e.g.* exploiting the substrate type). Moreover, this FR implies a learning ability of predators to optimize the encounter rate, such as specific predation strategies and the ability to focus preys' research in particular areas within the environment [58]. On the contrary, in the case of Holling type-II, prey's handling time is the mostly relevant issue, and indeed the presence of armors constitutes the preferred anti-predator tactic. When applied to the current analysis of the interaction between *P. turbinatus* and *C. erythropus*, the avoidance assumes a key role since the mollusk, being protected by a partial and thin armor, does not have sufficiently effective tools against predator's action. The hermit crab is indeed able to crack quite easily the mollusk's shell. Therefore, the mollusk is forced to adopt alternative defense strategies, such as escaping temporarily out of the water and taking refuge in certain places not accessible to predators.

In this context, mollusk shell plays a marginal role and it does not represent an engineering resource within the ecosystem. Also, it does not constitute an ideal foothold for other organisms such as epiphytes or epibionts. In fact, the *P. turbinatus* tends to move a lot during the day and to

get out of the water, making life on its shell very difficult for other organisms. On the contrary, shell remains fundamental for those bivalve molluscs that are almost motionless during their life and acts as a perfect substrate for other organisms [59].

Furthermore, as mentioned above regarding habitat structure, the FR describing crab predation on mollusks is also significantly affected by substrate type. Literature works [57, 60, 61] suggested that, in a substrate mostly made by pebbles and sand (as in beachrock pools), Holling type-III represents the most appropriate choice as it reflects the opportunity for preys of creating refuges and inaccessible habitats to predators.

In addition, Holling type-II is known to have more destabilizing effects and it can lead to localized extinction of preys at low density (see [30, 62]). We believe that this scenario is not applicable to our case as we've never detected, over the entire sampling period, the absence of *P. turbinatus*. On the contrary, Holling type-III has stabilizing effects and results in a low density refuge for preys. Holling type-III was also proposed as representative of the feeding behavior of predators in the presence of at least one alternative food source additional to the considered most relevant prey (see [56]). This is compatible with our observations, as we detected the presence of an alternative prey (*C. vulgatum*).

From the *mathematical* viewpoint, despite both type-II and III FRs allow to get, qualitatively, similar behaviors (such as the same number and typology of equilibria, the existence of periodic states), at least one key, substantial, difference between them has to be remarked. To highlight such a difference, we compare the bifurcation diagrams obtained in the two cases, reported in Figs.3 and A.1 (details on the calculations regarding the model (1) with Holling type-II FR are given in the Appendix). From the comparison between these figures, we notice that a qualitative agreement holds as a function of parameter k. In fact, in both cases, for $k < k_{min}$, no Hopf bifurcation is allowed (the state E_3^* is always stable in the whole domain) whereas, for $k \geq k_{min}$, Hopf bifurcation may arise (E_3^* can be destabilized by changes in the mortality parameter m). However, in this latter case, the most striking difference between the two FRs emerges. Indeed, in the model with Holling type-II, the range in which a limit cycle can be observed is localized close to the value of zero mortality, *i.e.* $m \in \left(0, m^H\right]$, with $m^H < m_{cr}$, as reported in eq.(A.4). In other words, this model would predict, for small values of predator's mortality, the existence of a periodic behavior instead of a (more likely) bloom of predators. On the contrary, in the case of Holling type-III, the Hopf range is located in a range far from predators' zero-mortality condition, *i.e.* $m \in \left[m_1^H, m_2^H\right]$, see eq.(11). This means that, for low values of m, predators' population is allowed to grow significantly giving rise to a recruitment peak, compatible with our observations in April 2017.

Therefore, from both ecological and mathematical viewpoints, the use of Holling type-III FR describes more closely the prey-predator dynamics observed *in situ*.

The presence of other species did not enter directly the model (1) due to their low average abundance, limited presence in time as well as a poor relevance on that trophic chain. In particular, the density of *C. vulgatum*, an alternative *C. erythropus*'s prey, was not here taken as an additional state variable. In fact, as already mentioned in Section 3.3, the role played by *C. vulgatum* during the whole observation period (15 months) is quite limited and restricted to less than 3 months (approximately January-April 2017). Outside this interval, this species was absent. The exceptional and isolated availability of this species has only contributed in a local (in time) decrease of predator's mortality rate which has favoured the occurrence of a second recruitment peak of predators not preceded by any prey's bloom (see the behavior reported in April 2017, Fig.7). As a further confirmation of the exceptional nature of the abundance of *C. vulgatum* in that temporal window, we performed an additional numerical study where mortality rate and carrying capacity exhibit periodicity over

time with given smooth functions (see Fig.11). Our numerical investigations confirmed that the only possibility to get a recruitment peak of the sole predators' population is to consider an aperiodic disturbance where the mortality rate is locally, but significantly, reduced.

Moreover, despite we do not expect significant interactions and competitions between the two preys (*P. turbinatus* and *C. vulgatum*), a more sophisticated model (accounting for two preys and a shared predator) may capture some additional details of this complex food web. This issue will be addressed in future developments of this work.

Thanks to the availability of data for each dynamical regime, the theoretical analysis was hence complemented by the identification of all model parameters. This procedure allowed to provide an estimation of some key quantities, that are generally not easily accessible (or even unknown) in the context of beachrock assemblage dynamics.

Moreover, numerical simulations were carried out with the twofold aim of validating our theoretical predictions and providing a deeper understanding on the complex dynamics here observed.

The proposed combined study, gathering *in situ* measurements and theoretical investigations, was mostly focused on acquiring a deeper understanding of the ecological processes ruling the interaction occurring in an oligotypic community in which few dominant elements are connected by clear trophic relationships. On the ecological side, we believe that our results may stimulate further developments to account for long-term dynamics and to inspect how these latter may be influenced by current climate changes. On the mathematical side, additional refinements of the model may include a network analysis [63, 64], to get information about the interactions among all the involved species, as well as the use of multipatch "stepping-stone" models [31, 65, 66] or continuous-dispersal models (leading to classical reaction-diffusion systems)[67], to account for an heterogeneous distribution of the populations over the beachrock enviroment.

5 Acknowledgements

G. Grifó and G. Consolo gratefully acknowledge support from INdAM-GNFM and from Italian MIUR through project PRIN2017 "Multiscale phenomena in Continuum Mechanics: singular limits, off-equilibrium and transitions"(project number: 2017YBKNCE).

A Appendix

In this Appendix we briefly summarize the key results obtained if the interaction between prey and predator were described through a Holling type-II response function:

$$h(P) = \frac{\lambda P}{\mu + P} \tag{A.1}$$

where the parameters λ and μ preserve the meaning defined in Section 2.5. Logistic growth and linear mortality rate are unchanged with respect to the previous case.

The mathematical model (1) with $h(P)$ given in (A.1) admits, formally, the same three equilibria found with Holling type-III, namely: $E_1^* = (0, 0)$, $E_2^* = (k, 0)$ and $E_3^* = (P_3^*, C_3^*)$ being

$$P_3^* = \frac{\mu m}{\lambda - m} \tag{A.2}$$

and

$$C_3^* = \frac{\beta}{m} P_3^* \left(1 - \frac{P_3^*}{k}\right). \tag{A.3}$$

We assume, again, the mortality-related parameter m and the carrying capacity k as main and secondary control parameters, respectively.

Results of linear stability analysis are qualitatively unchanged with respect to those obtained in the Holling type-III case. In fact, while the trivial state E_1^* and the predator-free state E_2^* exist for any set of parameter values, the co-existence state E_3^* is meaningful only if the parameter related to predator mortality m is smaller than the critical value $m_{cr} = \frac{\lambda k}{\mu + k}$. Moreover, the trivial state E_1^* is always unstable, while E_2^* is stable in the region of the control parameter where the coexistence state E_3^* does not exist. Regarding the stability of E_3^*, we find that it is asymptotically stable:

$$\begin{aligned} &\text{for } k < k_{min} \implies \text{always}, \\ &\text{for } k \geq k_{min} \implies \text{if } m \in \left(m^H, m_{cr}\right). \end{aligned} \tag{A.4}$$

being $k_{min} = \mu$ and $m^H = \frac{\lambda(k-\mu)}{k+\mu}$. At the critical value $m = m^H$, the state E_3^* becomes neutrally stable since eq.(6) admits a couple of complex-conjugate eigenvalues with null real part. For $0 < m < m^H$, the characteristic polynomial admits a couple of complex-conjugate roots with positive real part and, thus, the system undergoes a Hopf bifurcation. The bifurcation diagram resulting from the use of Holling type-II FR is depicted in Fig.A.1.

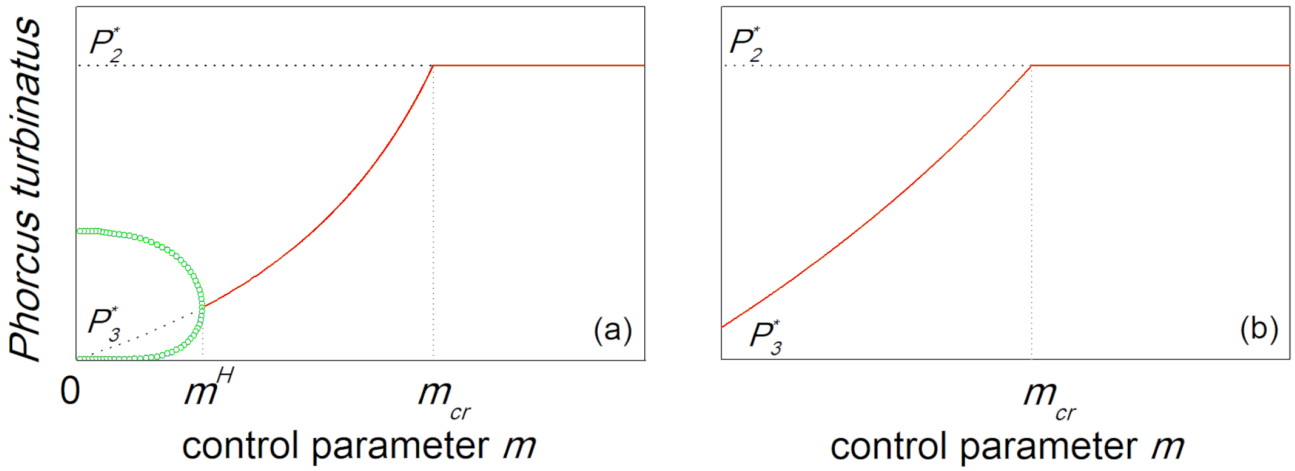

Figure A.1: Bifurcation diagrams for density P with m the main control parameter, $k \geq \mu$ in (a) and $k < \mu$ in (b). Circles denote stable periodic solutions whereas solid (dotted) lines represent stable (unstable) stationary solutions.

References

[1] Deangelis, D.L., Waterhouse, J.C. 1987. Equilibrium and nonequilibrium concepts in ecological models. Ecol. Monogr., 57(1), 1-21.

[2] Loreau, M. 2000. Biodiversity and ecosystem functioning: Recent theoretical advances. Oikos, 91(1), 3-17.

[3] Ortiz, M., Campos, L., Berrios, F., Rodriguez, F., Hermosillo, B., Gonzalez, J.. 2013. Network properties and keystoneness assessment in different intertidal communities dominated by two ecosystem engineer species (SE Pacific coast): A comparative analysis. Ecol. Model., 250, 307-318.

[4] Gabel, F., Stoll, S., Fisher, P., Pusch, M.T., Garcia, X.-F. 2011. Waves affect predator-prey interactions between fish and benthic invertebrates. Oecologia, 165, 101-109.

[5] Spanó, N. 1998. Distribution of crustacea decapoda (anomura and brachyura) in the straits of Messina. J. Nat. Hist., 32(10-11), 1697-1705.

[6] Spanó, N., De Domenico, E. 2017. Biodiversity in Central Mediterranean Sea. In Mediterr. Identities, IntechOpen 6, doi:10.5772/intechopen.68942.

[7] Cosentino, A., Giacobbe, S. 2015. Mollusc assemblages of hard bottom subtidal fringe: a comparison between two coastal typologies. Biol. J., 6(1), 353-364.

[8] Spurgeon, D., Davis Jr., R.A., Shinnu, E.A. 2003. Formation of Beach Rock' at Siesta Key, Florida and its influence on barrier island development. Mar. Geol., 200, 19-29.

[9] Al-Zamel, A., Al Sarkawi, M., and Khader, S. 2007. Coastal geomorphology, hydrodynamics, and biofacies in the intertidal and subtidal areas of Umm Al-Namil Island, Kuwait Bay, Kuwait. J. Coast. Res., 23, 501-514.

[10] Russell, R.J., McIntire, W.G. 1965. Southern Hemisphere Beach Rock. Geogr. Rev., 55, 17-45.

[11] Wainwright, S.A., Koehl, M.A.R. 1976. The nature of flow and the reaction of benthic Cnidaria to it, in: Coelenterate Ecology and Behavior. Springer, 5-21.

[12] Kelletat, D. 2006. Beachrock as Sea-Level Indicator Remarks from a Geomorphological Point of View. J. Coast. Res., 226, 1558-1564.

[13] Bottari, A., Bottari, C., Carveni, P., Giacobbe, S., Spanó, N. 2005. Genesis and geomorphologic and ecological evolution of the Ganzirri salt marsh (Messina, Italy). Quatern. Inter., 140141, 150-158.

[14] Vousdoukas, M.I., Velegrakis, A.F., Karambas, T.V. 2009. Morphology and sedimentology of a microtidal beach with beachroks: vatera, lesbos, NE Mediterranean. Cont. Shelf Res., 29, 1937-1947.

[15] Mauersberger, P. 1993. Intertidal and littoral ecosystems: A.C. Mathieson and P.H. Nienhuis (Editors). Ecosystems of the World 24, Elsevier, Amsterdam, 1991. Ecol. Model., 65(3), 306-307.

[16] Menge, B.A., Chan, F., Lubchenco, J. 2008. Response of a rocky intertidal ecosystem engineer and community dominant to climate change. Ecol. Lett., 11, 151-162.

[17] Wethey, D.S., Brin, L.D., Helmuth, B., Mislan, K.A.S. 2011. Predicting intertidal organism temperatures with modified land surface models. Ecol. Model., 222(19), 3568-3576.

[18] Xu, S., Chen, Z., Li, C., Huang, X., Li, S. 2011. Assessing the carrying capacity of tilapia in an intertidal mangrove-based polyculture system of Pearl River Delta, China. Ecol. Model., 222(3), 846-856.

[19] Gomes, P.B., Belm, M.J., Schlenz, E. 1998. Distribution, abundance and adaptations of three species of Actiniidae (Cnidaria, Actiniaria) on an intertidal beach rock in in Carneiros beach, Pernambuco, Brazil. Misc. Zool., 21(2), 65-72.

[20] Capillo, G., Panarello, G., Savoca, S., Sanfilippo, M., Albano, M., Li Volsi, R., Consolo, G., Spanó, N. 2018. Intertidal ponds of Messina's beachrock faunal assemblage, evaluation of ecosystem dynamics and communities' interactions. Atti Accad. Pelor. Peric. - Cl. Sci. Fis. Mat. Nat. 96(S3), A4.

[21] Abrams, P.A. 2019. The Evolution of Predator-Prey Interactions: Theory and Evidence. Ann. Rev. Ecol. Syst., 31, 79-105.

[22] Giacobbe, S., Renda, W. 2018. Mollusc diversity in Capo d'Armi (Central Mediterranean Sea) subtidal cliff: a first, tardy, report. Biol. J., 9(1), 25-34.

[23] Battaglia, P., Pagano, L., Consoli, P., Esposito, V., Granata, A., Guglielmo, L., Pedá, C., Romeo, T., Zagami, G., Vicchio, T.M., Guglielmo, R., Andaloro, F. 2020. Consumption of mesopelagic prey in the Strait of Messina, an upwelling area of the central Mediterranean Sea: feeding behaviour of the blue jack mackerel *Trachurus picturatus* (Bowdich, 1825). Deep-Sea Res. Part I: Ocean. Res. Papers, 155, 103158.

[24] Ingrosso, G., Abbiati, M., Badalamenti, F., Bavestrello, G., Belmonte, G., Cannas, R., Benedetti-Cecchi, L. et al. 2018. Mediterranean bioconstructions along the Italian coast. Adv. Mar. Biol., 79, 61-136.

[25] Capillo, G., Savoca, S., Costa, R., Sanfilippo, M., Rizzo, C., Giudice, A. Lo, Albergamo, A., Rando, R., Bartolomeo, G., Spanó, N., Faggio, C. 2018. New insights into the culture method and antibacterial potential of gracilaria gracilis. Mar. Drugs, 16(12), 492.

[26] Sanfilippo, M., Capillo, G., Spanó, N., Manganaro, A. 2016. Evaluation of water variables in no-take zone of Ustica marine protected area (Southern Tyrrhenian Sea). Brazilian Arch. Biol. Technol., 59, e16160330.

[27] Mangano, M.C., Kaiser, M.J., Porporato, E.M.D., Lambert, G.I., Spanó, N. 2015. Trawling disturbance effects on the trophic ecology of two co-generic Astropectinid species. Mediterr. Mar. Sci., 16(3), 538-549.

[28] Hammer-Muntz, O., Harper, D., Ryan, P. 2001. PAST-palaeontological statistics, ver. 1.89. Palaeontol. Electron., https://folk.uio.no/ohammer/past/.

[29] Barbera, E., Consolo, G., Valenti, G. 2015. A two or three compartments hyperbolic reaction-diffusion model for the aquatic food chain. Math. Biosci. Eng., 12(3), 451-472.

[30] Holling, C.S. 1959. The components of predation as revealed by a study of small-mammal predation of the european pine sawfly. The Canad. Entomol., 91, 293-320.

[31] Levy, D., Harrington, H. A., VanGorder, R. A. 2016. Role of seasonality on predator-prey-subsidy population dynamics. J. Theor. Biol., 396, 163-181.

[32] Jansen, J. E., Van Gorder, R. A. 2018. Dynamics from a predator-prey-quarry-resource-scavenger model. Theor. Ecol., 11, 19-38.

[33] Fitzgerald, C.J., Shephard, S., McLoone, P., Kelly, F.L. and Farnsworth, K.D. 2019. Evaluating management options for two fisheries that conflict through predator-prey interactions of target species. Ecol. Model., 410, 108740.

[34] Costa, M.I.D.S. and dos Anjos, L. 2018. Multiple hydra effect in a predator-prey model with Allee effect and mutual interference in the predator. Ecol. Model., 373, 22-24.

[35] Caruso, T., Chemello, R. 2009. The size and shape of shells used by hermit crabs: A multivariate analysis of *Clibanarius erythropus*. Acta Oecologica, 35(3), 349-354.

[36] Tricarico, E., Bertocchi, S., Brusconi, S., Chessa, L.A., Gherardi, F. 2009. Shell recruitment in the Mediterranean hermit crab *Clibanarius erythropus*. J. Exp. Mar. Biol. Ecol, 381(1), 42-46.

[37] Chapman, E.J., Byron, C.J. 2018. The flexible application of carrying capacity in ecology. Glob. Ecol. Conserv., 13, e00365.

[38] Yodzis, P. 1989. Introduction to theoretical ecology. Harper & Row, Publishers, New York.

[39] Consolo, G., Valenti, G. 2019. Secondary seed dispersal in the Klausmeier model of vegetation for sloped semi-arid environments. Ecol. Model., 402, 66 - 75.

[40] Ermentrout, B. 2002. Simulating, Analyzing, and Animating Dynamical Systems: A Guide to XPPAUT for Researchers and Students (Software, Environments and Tools). SIAM.

[41] Nott, J.A., Nicolaidou, A. 1994. Variable transfer of detoxified metals from snails to hermit crabs in marine food chains. Mar. Biol., 120, 369-377.

[42] Benvenuto, C., Gherardi, F. 2001. Population structure and shell use in the hermit crab, *Clibanarius erythropus*: A comparison between Mediterranean and Atlantic shores. J. Mar. Biol. Assoc. U. K., 81(1), 77-84.

[43] Pérez-Miguel, M., Cuesta, J.A., Manzano, R., Drake, P. 2016. Sex- and size-related differences in shell use by the intertidal hermit crab *Clibanarius erythropus* (Latreille, 1818) (Decapoda: Diogenidae) in the Gulf of Cadiz, southwestern Spain. J. Crustac. Biol., 36(1), 23-32.

[44] Milazzo, M., Badalamenti, F., Riggio, S., Chemello, R. 2004. Patterns of algal recovery and small-scale effects of canopy removal as a result of human trampling on a Mediterranean rocky shallow Community. Biol. Cons., 117(2), 191-2020.

[45] Mosbahi, N., Pezy, J.-P., Dauvin, J.-C., Neifar, L. 2016. Spatial and Temporal Structures of the Macrozoobenthos from the Intertidal Zone of the Kneiss Islands (Central Mediterranean Sea). Open J. Mar. Sci., 6(2), 223-237.

[46] Chaouti, A., Bayed, A. 2017. Seasonal patterns of the macrozoobenthic community structure according to environmental conditions in a western Mediterranean lagoon close to the Gibraltar strait. J. Mater. Environ. Sci., 8, 2921-2931.

[47] Trowbridge, C.D., 1994. Life at the edge: population dynamics and salinity tolerance of a high intertidal pool-dwelling ascoglossan opisthobranch on New Zeland rocky shores. J. Exp. Mar. Biol. Ecol., 182, 65-84.

[48] Gonzalez, R.J. 2012. The physiology of hyper-salinity tolerance in teleost fish: a review. J. Comp. Physiol. B Biochem. Syst. Environ. Physiol., 182(3), 321-329.

[49] Al-Maslamani, I., Al-Masdi, A., Smyth, D.M., Chatting, M., Obbard, J.P., Giraldes, B.W. 2015. Baseline monitoring gastropods in the intertidal zone of Qatar-target species and bioindicators for hyper-thermic and hyper-saline conditions. Int. J. Res. Stud. Biosci., 3(12), 62-72

[50] Chomsky, O., Kamenir, Y., Hyams, M., Dubinsky, Z., Chadwick-Furman, N.E. 2004. Effects of temperature on growth rate and body size in the Mediterranean Sea anemone *Actinia equina*. J. Exp. Mar. Biol. Ecol., 313(1), 63-73.

[51] Sheaves, M., Dingle, L., Mattone, C. 2016. Biotic hotspots in mangrove-dominated estuaries: Macro-invertebrate aggregation in unvegetated lower intertidal flats. Mar. Ecol. Prog. Ser., 556, 31-43.

[52] Schifano, G., 1983. Allometric growth as influenced by environmental temperature in Monodonta turbinata shells. Palaeogeogr. Palaeoclimatol. Palaeoecol., 44(3-4), 215-222.

[53] Sousa, R., Delgado, J., Gonzalez, J.A., Freitas, M., Henriques, P. 2018. Marine Snails of the Genus Phorcus: Biology and Ecology of Sentinel Species for Human Impacts on the Rocky Shores, in Biological Resources of Water. IntechOpen., 7.

[54] Steele, J. H., Henderson, E. W. 1992, A simple model for plankton patchiness. J. Plank. Res., 14, 1397-1403.

[55] Truscott, J.E., Brindley, J. 1994. Ocean plankton populations as excitable media, Bull. Math. Biol., 56, 981-998.

[56] Brentnall, S. J., Richards, K. J., Brindley, J., Murphy, E. 2003. Plankton patchiness and its effect on larger-scale productivity. J. Plank. Res., 25(2), 20-41.

[57] Seitz, R. D., Lipcius, R. N., Hines, A. H., Eggleston, D. B. 2001. Density-dependent predation, habitat variation, and the persistence of marine bivalve prey. Ecology, 82(9), 2435-2451.

[58] Dawes, J. H. P., Souza, M. O. 2013. A derivation of Holling's type I, II and III functional responses in predator-prey systems. J. Theor. Biol., 327, 11-22.

[59] Gutiérrez, J.L., Jones, C.G., Strayer, D.L. and Iribarne, O.O. 2003. Mollusks as ecosystem engineers: the role of shell production in aquatic habitats. Oikos, 101, 79-90.

[60] Sponaugle, S., Lawton, P. 1990. Portunid crab predation on juvenile hard clams: effects of substrate type and prey density. Mar. Ecol. Progr. Ser., 67, 43-53.

[61] Boulding, E.G., Hay, T.K. 1984. Crab response to prey density can result in density-dependent mortality of clams. Can. J. Fish. Aquat. Sci., 41, 521-525.

[62] Rindone, R. R., Eggleston, D. B. 2011. Predator-prey dynamics between recently established stone crabs (Menippe spp.) and oyster prey (Crassostrea virginica). J. Exp. Mar. Biol. Ecol., 407, 216-225.

[63] Montoya, J. M., Pimm, S. L., Solé, R. V. 2006. Ecological networks and their fragility. Nature, 442, 259-264.

[64] Poisot, T., Stouffer, D. B., Kéfi, S. 2016. Describe, understand and predict: why do we need networks in ecology?. Funct. Ecol., 30, 1878-1882.

[65] Shen, L., Van Gorder, R. A. 2017. Predator-prey-subsidy population dynamics on stepping-stone domains. J. Theor. Biol., 420, 241-258.

[66] Fussell, E. F., Krause, A. L., Van Gorder, R. A. 2019. Hybrid approach to modeling spatial dynamics of systems with generalist predators. J. Theor. Biol., 462, 26-47.

[67] Bassett, A., Krause, A.L. and Van Gorder, R.A. 2017. Continuous dispersal in a model of predator-prey-subsidy population dynamics. Ecol. Model., 354, 115-122.